Natural variants in *C. elegans atg-5* 3'UTR uncover divergent effects of autophagy on polyglutamine aggregation in different tissues

Alexander-Floyd J[1], Haroon S[2], Ying M[1], Entezari AA[1,3], Jaeger C[1,4], Vermulst M[2,5], Gidalevitz T[1,#].

[1] Biology Department, Drexel University, Philadelphia, PA 19104

[2] Department of Pathology and Laboratory Medicine, Children's Hospital of Philadelphia, Philadelphia, PA 19104

[3]Current address: Department of Pathology, Anatomy and Cell Biology, Thomas Jefferson University, Philadelphia, PA 19107

[4]Current address: Department of Neuroradiology, Technical University of Munich, Munich, Germany

TUM-Neuroimaging Center, Technical University of Munich, Munich, Germany

[5]Current address: Leonard Davis School of Gerontology, University of Southern California, Los Angeles, CA 90089

[#] Corresponding author. Address correspondence to T.G. (tg443@drexel.edu)

Short title: Divergent effects of autophagy on polyglutamine aggregation in different tissues

Abstract

Diseases caused by protein misfolding and aggregation, in addition to cell selectivity, often exhibit variation among individuals in the age of onset, progression, and severity of disease. Genetic variation has been shown to contribute to such clinical variation. We have previously found that protein aggregation-related phenotypes in a model organism, *C. elegans*, can be modified by destabilizing polymorphisms in the genetic background and by natural genetic variation. Here, we identified a large modifier locus in a Californian wild strain of *C. elegans*, DR1350, that alters the susceptibility of the head muscle cells to polyglutamine (polyQ) aggregation, and causes an increase in overall aggregation, without changing the basal activity of the muscle proteostasis pathways known to affect polyQ aggregation. We found that the two phenotypes were genetically separable, and identified regulatory variants in a gene encoding a conserved autophagy protein ATG-5 (ATG5 in humans) as being responsible for the overall increase in aggregation. The *atg-5* gene conferred a dosage-dependent enhancement of polyQ aggregation, with DR1350-derived *atg-5* allele behaving as a hypermorph. Examination of autophagy in animals bearing the modifier locus indicated enhanced response to an autophagy-activating treatment. Because autophagy is known to be required for the clearance of polyQ aggregates, this result was surprising. Thus, we tested whether directly activating autophagy, either pharmacologically or genetically, affected the polyQ aggregation in our model. Strikingly, we found that the effect of autophagy on polyQ aggregation was tissue-dependent, such that activation of autophagy decreased polyQ aggregation in the intestine, but increased it in the muscle cells. Our data show that cryptic genetic variants in genes encoding proteostasis components, although not causing visible phenotypes under normal conditions, can have profound effects on the behavior of aggregation-prone proteins, and suggest that activation of autophagy may have divergent effects on the clearance of such proteins in different cell types.

Introduction

Protein misfolding and aggregation underlie many human diseases, and contribute to tissue decline during aging (1, 2). In hereditary neurodegeneration, the disease-causing mutations are often directly responsible for misfolding and aggregation of the mutant protein (3, 4). For example, expansions of the CAG repeats in several different diseases lead to expanded polyglutamine (polyQ) tracts in affected proteins, which in turn result in their increased aggregation propensity (5-7). Such mutations exhibit "toxic gain-of-function" behavior, and thus a dominant, monogenic inheritance pattern. How misfolding or aggregation of these proteins cause the gain-of-function toxicity, and why they lead to disease is still incompletely understood. Two aspects of protein aggregation diseases may contribute to this difficulty. First, the behavior of mutant proteins appears to depend on the cellular environment: although they are often expressed broadly or even ubiquitously, only select subsets of cells are affected in each disease (8). The reasons for such differential susceptibility could lay in specific characteristics of the susceptible cells, such as for example the possible contribution of dopaminergic pathways in Parkinson's disease; however, in most cases, the causes are unknown (8, 9). Second, while monogenic, these diseases show variation in the age of onset, severity, or clinical phenotypes (10). The variation is thought to result from stochastic and environmental factors, and from variants present in individual's genetic background that act as modifiers (11-13). These genetic modifiers can affect proteins and regulatory pathways that either interact with the disease-causing mutant proteins, or are themselves impacted in disease (14). For example, modifiers of age of onset act prior to the onset of clinical manifestations and as such are expected to affect processes involved in the early pathogenic steps. Therefore, identifying natural modifier variants and their mechanisms can expand our understanding of cellular pathways involved in disease. Natural variants may also indicate pathways that differ from those found by the traditional approaches, such as association studies, mutagenesis, or RNAi screens. Importantly, because such modifiers are a part of natural genetic variation and are present in phenotypically normal individuals, they may pinpoint therapeutic routes that are less likely to cause detrimental side effects.

The most informative way to map genetic modifiers of disease is directly in human patients (13). A number of studies have shown that variants in genes other than the polyQ-expanded huntingtin (Htt) are capable of modifying the pathogenesis of Huntington's Disease (HD) (12, 15-18). Two recent large studies of modifiers of the age of onset of HD have identified four loci on Chromosomes 3, 8 and 15 in HD subjects of European ancestry, and a locus on Chromosome

7 in a Venezuelan HD cluster (19-21). Pathway analysis implicated DNA repair pathways in European HD as having modifying effects, possibly via changing the size of the CAG repeat in somatic tissues, while the modifier locus in Venezuelan HD may act by regulating the bone morphogenetic protein (BMP) signaling. However, the causal genes and mechanisms involved are still unknown (19-21). The difficulties in using human patients in search for modifiers across aggregation diseases include the size and complexity of the human genome, the often small size of affected populations, and the possibility for the complex interactions among multiple modifiers (10, 13, 22). In addition, human studies may have limited ability to identify modifiers that are rare, or segregate in families rather than in entire affected populations. Model organisms offer a genetically tractable alternative due to the evolutionary conservation of the main cellular pathways. Expression of disease-related proteins in these organisms recapitulate many characteristics of human diseases that are related to the basic biology of protein misfolding and aggregation (23). For example, *C. elegans* and *Drosophila* models expressing polyQ-expanded Htt or ataxin-3, or isolated polyglutamine repeats, exhibit similar toxic gain-of-function behavior and the age- and polyQ-length dependent aggregation and toxicity as those seen in patients and in mammalian models (24-34). Many candidate modifying pathways identified in model organisms proved to be conserved, including insulin signaling, the heat-shock response, or regulators of proteostasis (35). Importantly, as in human disease, polyQ expansions in *C. elegans* also exhibit dependence on both the cellular environment (30, 36, 37) and the genetic background (38), despite their dominant gain-of-function behavior. We have previously shown that genetic variants coding for marginally stable proteins, although innocuous under normal conditions, can dramatically change both the aggregation and the associated toxicity of the aggregation-prone proteins, suggesting that genetic variation may directly impinge on cellular proteostasis (37, 39). Indeed, introduction of natural variation into the genetic background of polyQ-expressing animals independently modified several different aspects of polyQ behavior, including the onset and extent of aggregation, the susceptibility of different types of muscle cells to aggregation, and the resulting loss of motility and shortened lifespan (38). The polyQ aggregation in these genetically variable animals showed transgressive segregation, indicating that multiple additive or interacting alleles in parental backgrounds were acting as modifiers (38). A recent study has shown that natural variation also modulates the phenotypes and transcriptional changes caused by expression of α-synuclein transgene in the body-wall muscle cells of *C. elegans* (40). Thus, natural genetic variation within *C. elegans* wild strains can be used to investigate the mechanisms and pathways controlling the toxic effects of protein

misfolding and aggregation.

Here, we dissected the genetic variation causing increased aggregation of the muscle-expressed 40-residue polyQ expansion (Q40::YFP, or Q40) in the background of a Californian wild strain of *C. elegans*, DR1350 (38). We identified a large modifier locus on Chromosome I as being causal for two phenotypes: altered susceptibility of the head muscle cells to aggregation and increased overall aggregation. These phenotypes were genetically separable, and we identified regulatory variants in a gene encoding a conserved autophagy protein ATG-5 as being responsible for the latter phenotype. The *atg-5* gene conferred a dosage-dependent enhancement of polyQ aggregation, with DR1350-derived *atg-5* allele behaving as a hypermorph. Surprisingly, animals bearing the variant *atg-5* allele showed enhanced response to an autophagy-activating drug. Because autophagy is expected to clear polyQ aggregates, we tested the effect of directly activating autophagy on the polyQ aggregation in our model, and found a striking tissue-dependence for the effect of autophagy on polyQ aggregation. Our data show that cryptic genetic variants in genes encoding proteostasis components can have profound effects on the behavior of aggregation-prone proteins, and suggest that activation of autophagy may have divergent effects on the clearance of such proteins in different cell types.

Results

DR1350-derived variants increase polyglutamine aggregation

We previously found that introgression of an integrated polyglutamine-encoding transgene (Q40) from the laboratory Bristol/N2 background (Q40Bristol) into the wild California isolate DR1350 resulted in strongly accelerated polyglutamine aggregation in the body-wall muscle cells, and a characteristic increase in the relative susceptibility of the normally resistant head muscle cells to polyQ aggregation (38). These two phenotypes were also present in 5 out of 21 recombinant inbred lines (RILs) derived from a cross between Q40Bristol and Q40DR1350 strains (38). To isolate the genetic variation that contributed to increased aggregation, we chose one (RIL2) that exhibited more than 2-fold increase in the number of aggregates relative to the Q40Bristol parent at the late fourth larval stage (L4) (**Fig. 1A**). We backcrossed RIL2 animals to the Q40Bristol parental strain 23 times, selecting for the F2 progeny that inherited RIL2-like phenotypes after each round of backcrossing (**Fig. 1B**). This approach ensured that the DR1350-derived RIL2 variants that contributed to the polyQ phenotypes were retained in the resulting 23x backcrossed strain, while the majority of its background was derived from the Q40Bristol parental strain. The backcrossed strain is referred to as *drxIR1*;Q40 (**Fig. 1B**). Since the

increased susceptibility of the head muscles is an easy to detect qualitative phenotype that behaved in our RIL panel as a recessive trait (38), we used this phenotype during F2 progeny selection. Interestingly, the *drxIR1*;Q40 strain also retained the second polyQ phenotype - the increased overall aggregation **(Fig. 1A**), suggesting that the two phenotypes result from either linked or same natural variant(s). Age-matched *drxIR1*;Q40 animals had a higher number of polyQ40 aggregates than Q40Bristol until day 2 of adulthood, when polyQ40 aggregation reached its maximum in both strains (**Fig. 1C**). Thus, natural variants present in the wild isolate DR1350 can modify polyglutamine aggregation when introgressed into the Bristol genetic background.

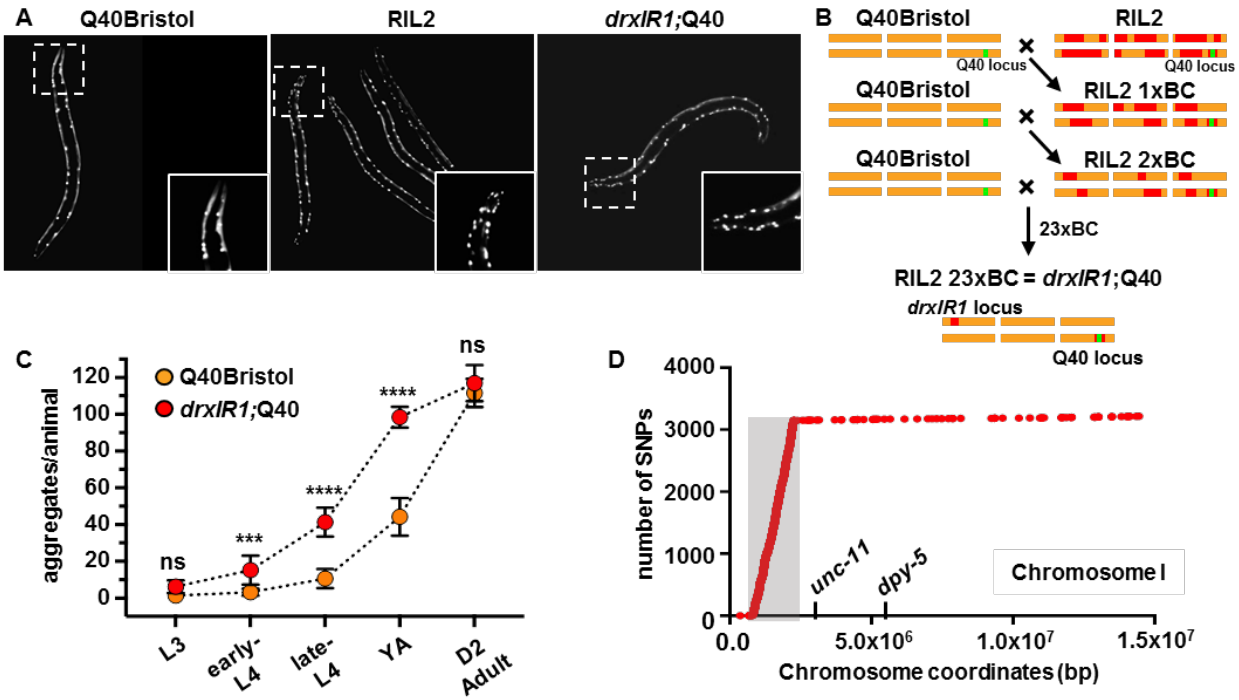

Fig 1. *drxIR1* locus causes increased polyQ40 aggregation.

(**A**) Late-L4 RIL2 and *drxlR1*;Q40 animals have increased aggregation compared to Q40Bristol animals. (**B**) The scheme for generation of the *drxIR1*;Q40 strain through rounds of crossing-selection. RIL2 strain was backcrossed (**BC**) into the Q40Bristol strain 23 times. DR1350-derived variants that are retained through the crossing-selection scheme are those contributing to the RIL2 polyQ phenotype (and their linked variants). (**C**) The *drxIR1*;Q40 animals exhibit a faster accumulation of polyQ aggregates compared to Q40Bristol at all developments stages, until both strains reach maximum at Day 2 of adulthood. L3, L4, YA and D2 adult indicate 3rd and 4th larval stage, young adult, and day 2 adult stage, respectively. Data are mean ± SD, 10 to 20 animals per data point. Data were analyzed by ANOVA followed by Bonferroni's multiple comparison test, ****P<0.0001, ***P=0.0004. **Orange**:

Q40Bristol background, **red**: *drxIR1*;Q40. Same color scheme is used in all figures. (**D**) DR1350-derived locus with over 3000 unique SNPs (in the grey-shaded area) to the left of *unc-11* on Chromosome I in *drxIR1*;Q40 strain.

Polyglutamine aggregation-modifying variants reside in a large interval inherited from the DR1350 parent

In order to identify the causative variant(s) in the backcrossed *drxIR1*;Q40 strain, we first used mapping strains with visible mutations on each Chromosome, and found that increased aggregation segregated with the left arm of Chromosome I. This location was confirmed (described further below) using a free duplication sDP2 (41), which covers the left arm of Chromosome I through *dpy-5* (**Suppl. Table 1**). To precisely map the variant(s), we performed genome sequencing of both the *drxIR1*;Q40 and Q40Bristol strains and identified SNPs present only in the former, using Galaxy pipeline described in (42). We found that the left arm of Chromosome I in the backcrossed *drxIR1*;Q40 strain contained an 1.43Mb interval (ChrI:832,674-2,262,484), with over 4,000 SNPs. Because our previous data showed that introgression of the Q40 transgene into the commonly used CB4856 (Hawaiian) strain did not result in the same aggregation phenotypes as in the DR1350 background (38), we further subtracted the known Hawaiian SNPs (43) and found that the interval still contained over 3,000 SNPs (**Fig. 1D**). We tested whether this interval was also present in the remaining four high-aggregation RILs from the original study, by following several SNPs within the interval (**Suppl. Fig. 1**). We found that three of the RILs indeed inherited the entire interval, while the interval in the fourth one (RIL15) was shorter on the right side, extending through SNP 6 at ChrI:1,850,249 (WBVar00017051), but not through SNP 6b at ChrI:1,972,719 (WBVar00017376) (**Suppl. Fig. 1**). Thus, four independent RILs with high polyQ aggregation phenotypes, and the 23 times back-crossed *drxIR1*;Q40 strain derived from another RIL (RIL2), all contained the parental interval ChrI:832,674-1,972,719 from the high-aggregation DR1350;Q40 strain. To confirm, we used a mutation in *egl-30* gene located within this interval (**Suppl. Fig. 1**). We were unable to find any F2 progeny from 10 F1 heterozygotes from a cross between *drxIR1*;Q40 and *egl-30(n686)* animals that showed both the RIL2-like polyQ head aggregation phenotype and the *egl* phenotype (>1000 F2s), consistent with a close genetic linkage. Furthermore, in subsequent genetic crosses between *drxIR1*;Q40 and Q40;Bristol animals, we observed a complete correlation between F2 progeny inheriting two copies of this interval, as detected by following SNP 5 (WBVar00016276) (see Methods), and the appearance of the two polyQ phenotypes

(>100 animals). Together, these data indicate that ChrI:832,674-1,972,719 interval is responsible for increased polyQ aggregation phenotypes.

The remaining part of Chromosome I contained 68 additional SNPs relative to the Q40Bristol parental strain, and all the other Chromosomes accumulated less than 200 unique SNPs each (**Suppl. Fig. 2**), consistent with previous reports (44). The large size of the modifier interval was unexpected after 23 backcrosses, suggesting that it may contain structural variants preventing recombination over this region. Alternatively, this locus could contain more than one SNP responsible for the phenotypes, perhaps distributed over the interval. Of note, the known Chromosome I *zeel-1*/*peel-1* incompatibility locus (45) was not responsible for the retention of the modifier interval through the backcrosses, as it lays outside the mapped interval (**Suppl. Fig. 1**), and does not contain DR1350-derived SNPs in the *drxIR1*;Q40 strain.

Known regulators of proteostasis are not responsible for increased polyQ aggregation in *drxIR1* animals

Because the identified modifier locus contained a large number of SNPs, we thought to narrow down the candidate pathway(s) in which the modifier gene(s) acted. We first asked whether the variants in the *drxIR1* locus were increasing polyglutamine aggregation by affecting either the protein homeostasis of the muscle cells, or the Q40::YFP protein itself. We have previously tested and excluded the trivial explanation that the increased aggregation in our five RILs was due to the increased expression of the Q40::YFP protein (38). Nonetheless, we considered a possibility that *drxIR1* locus could cause increased activity of the *unc-54* promoter that was used to drive the polyglutamine transgene. To test this, we introduced an integrated *unc-54p*::GFP::UNC-54 transgene (46) into the *drxIR1* background, in the absence of polyQ, and examined its expression. We found no differences in the fluorescence levels, suggesting normal *unc-54* promoter activity (**Fig. 2A**). Since assembly of myofilaments is sensitive to both the levels of UNC-54 myosin heavy chain protein and the activity of molecular chaperones, it provides an additional measure of the GFP::UNC-54 protein levels and of the folding environment (47-49). We found normal striated pattern of GFP::UNC-54 protein in both Bristol and *drxIR1* genetic backgrounds (**Fig. 2B**).

Another reason for increased aggregation could be decreased protein turnover. To address this, we asked whether basal autophagy or proteasome activity were reduced in the muscle cells of *drxIR1* animals. Using a well-characterized autophagy reporter ubiquitously expressing GFP::LGG-1 (50), GFP::LGG-1 puncta were counted in the muscle cells of wild type and *drxIR1*

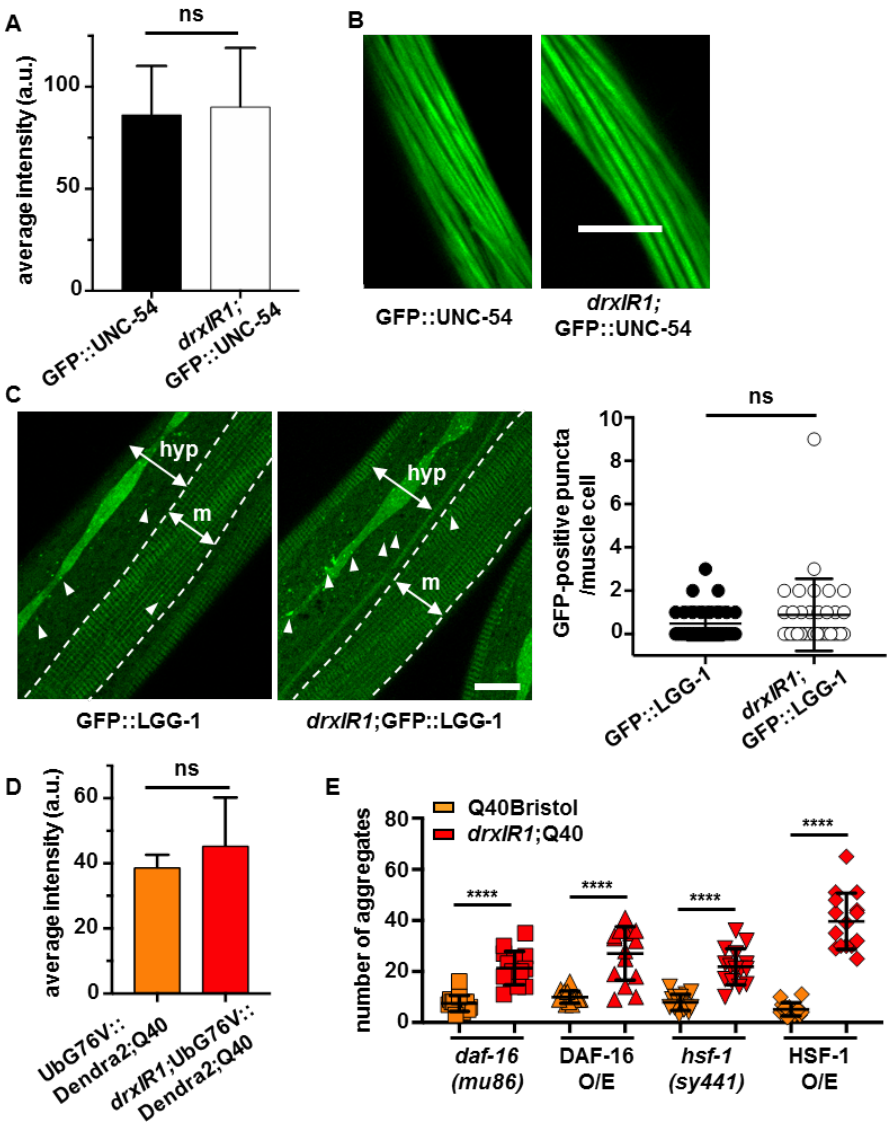

Fig 2. Basal protein homeostasis of muscle cells is unaffected in animals carrying the *drxIR1* interval.

(**A**) Expression of GFP::UNC-54 fusion protein from *unc-54* promoter is similar between the Bristol and *drxIR1* L4 animals. Data are mean ± SD of GFP fluorescence intensity, 16-20 muscle cells per genotype, unpaired *t*-test, two-tailed. (**B**) Myofilament assembly is normal in *drxIR1* animals. Confocal images of muscle cells. Scale bar: 10 μm. (**C**) Muscle cells have very few GFP::LGG-1-positive puncta (**arrowheads**) in both Bristol and *drxIR1* L4 animals. One muscle quadrant is shown between punctate lines. **m**: muscle, **hyp**: hypodermis. An increased number of GFP::LGG-1-positive puncta is seen in the hypodermis of *drxIR1*. Scale bar is 10 μm. Right panel, quantification of GFP::LGG-1 puncta in the muscle cells. Data are mean ± SD, 30 to 40 cells (8 to 10 animals) per genotype, unpaired *t*-test, two-tailed; each symbol represents individual cells. (**D**) No difference in the average intensity of the proteasome reporter fluorescence in Q40Bristol and *drxIR1*;Q40 animals. Data are mean ± SD, 4-5 animals, unpaired *t*-test, two-tailed. (**E**) The increased aggregation phenotype in

animals carrying the *drxlR1* interval does not depend on DAF-16 or HSF-1. Each symbol represents an individual animal, 15 mid-L4 animals per genotype. **O/E**: overexpression. Means ± SD are overlaid. Data were analyzed by ANOVA followed by Bonferroni's multiple comparison test, ****P<0.0001.

animals, in the absence of the Q40::YFP protein to avoid spectral overlap. Consistent with previously published results, the number of GFP-positive puncta in the muscle cells of L4 animals with the Bristol background was low (51, 52), and we detected no difference in basal autophagy in the muscle cells of *drxIR1* animals (**Fig. 2C**), although increased number of puncta was noted in their lateral hypodermis. To test whether decreased proteasomal activity could be responsible for the increased aggregation seen in the *drxIR1*;Q40 animals, we introduced a muscle specific UbG76V::Dendra2 reporter (53) into Q40Bristol and *drxIR1;*Q40 animals, and measured its fluorescence. We detected no increase in Dendra2 fluorescence in *drxIR1* animals, indicating that there was no decrease in the proteasome activity (**Fig. 2D**). To confirm that the reporter was sensitive to decreased proteasome activity, we reduced expression of the *rpn-6.1* subunit of 19S regulatory complex of the proteasome *via* RNAi (53) and detected an increase in Dendra2 fluorescence (**Suppl. Fig. 3A**). These data indicate that increased polyglutamine aggregation in the muscle cells of *drxIR1* animals is not due to the changes in protein degradation or in polyQ protein levels.

Next, we tested two main transcriptional pathways known to regulate cytosolic protein homeostasis - insulin signaling and the heat-shock response. Increased activity of DAF-16/FOXO, the transcription factor of the insulin signaling pathway, is associated with improved proteostasis and has been shown to affect polyglutamine aggregation (30, 36). We found that neither genetic inactivation of *daf-16*, using *daf-16(mu86)* mutation (54), nor overexpression of active DAF-16::GFP protein (55), were able to revert the increased aggregation seen in *drxIR1;*Q40 animals (**Fig. 2E**). HSF-1/HSF1 is the heat shock transcription factor that functions as a master regulator of molecular chaperones, degradation machinery, and other proteostasis components in the cytosol, and has also been shown to affect polyQ aggregation in wild type animals (36). Similarly to DAF-16, neither the hypomorphic *hsf-1(sy441)* allele, deficient in the heat-shock response (56), nor HSF-1 overexpression (57), were able to revert the increased aggregation caused by *drxIR1* background (**Fig. 2E**). Together, these data indicate that the DR1350-derived variants in *drxIR1* are not likely to act by modifying the basal proteostasis of the muscle cells of *C. elegans*.

Variants in the introgressed interval do not alter biophysical properties of polyQ40 aggregates

Besides changes in the cellular proteostasis of the muscle cells, the increased aggregation in *drxIR1*;Q40 animals could reflect changes in the amyloid-like nature and/or biophysical properties of polyQ40 aggregates themselves. PolyQ40 is known to form immobile aggregates that do not recover after photobleaching, and are resistant to treatment with the detergent SDS (30, 58). Thus, we tested whether the presence of *drxIR1* interval altered these properties of polyQ40 aggregates. As expected, photobleaching foci within Q40Bristol resulted in essentially no recovery of fluorescence, while soluble Q40::YFP protein rapidly recovered to pre-bleach levels (**Fig. 3A**). We found no difference in recovery of Q40::YFP foci between *drxIR1*;Q40 and Q40Bristol animals (**Fig. 3A**), indicating similarly immobile aggregates. To test for SDS resistance, we extracted aggregates from Q40Bristol and *drxIR1*;Q40 animals and treated them with 5% SDS at room temperature, as described in (39). We found polyQ aggregates to be similarly SDS resistant in both genetic backgrounds (**Fig. 3B**). To confirm that our SDS treatment could dissociate non-amyloid protein assemblies, we tested GFP::UNC-54 protein that forms myofilaments (as shown in Fig. 2B). Filamentous GFP::UNC-54 protein was efficiently dissociated by SDS treatment in extracts from both Bristol and *drxIR1* backgrounds (**Fig. 3B**). recently discovered positive regulator of aggregation, MOAG-4/SERF, which specifically distinguishes amyloid and non-amyloid aggregation (59, 60), was shown to affect Q40::YFP protein in *C. elegans*. Decrease of *moag-4* expression *via* RNAi suppresses aggregation of polyglutamine, amyloid-beta (Aβ), and α-synuclein, but not of mutant SOD1 (60). To test whether the variants in the *drxIR1* background act through MOAG-4, expression of *moag-4* was knocked down by RNAi in Q40Bristol and *drxIR1*;Q40 animals. *moag-4* RNAi strongly decreased polyQ40 aggregation in both backgrounds, confirming the amyloid-like nature of aggregation in both (**Fig. 3C** (L4 animals) and **Suppl. Fig. 3B** (young adults)). However, *drxIR1*;Q40*;moag-4*(RNAi) animals retained higher aggregation relative to Q40Bristol*;moag-4*(RNAi) animals (**Fig. 3C**), as well as the increased susceptibility of the head muscles (**Suppl. Fig. 3B**), arguing against the *drxIR1* interval variants acting through MOAG-4-mediated mechanism. Together our data suggest that neither decrease in muscle proteostasis nor changes in the aggregation pathway are responsible for the increased aggregation in *drxIR1*;Q40 animals.

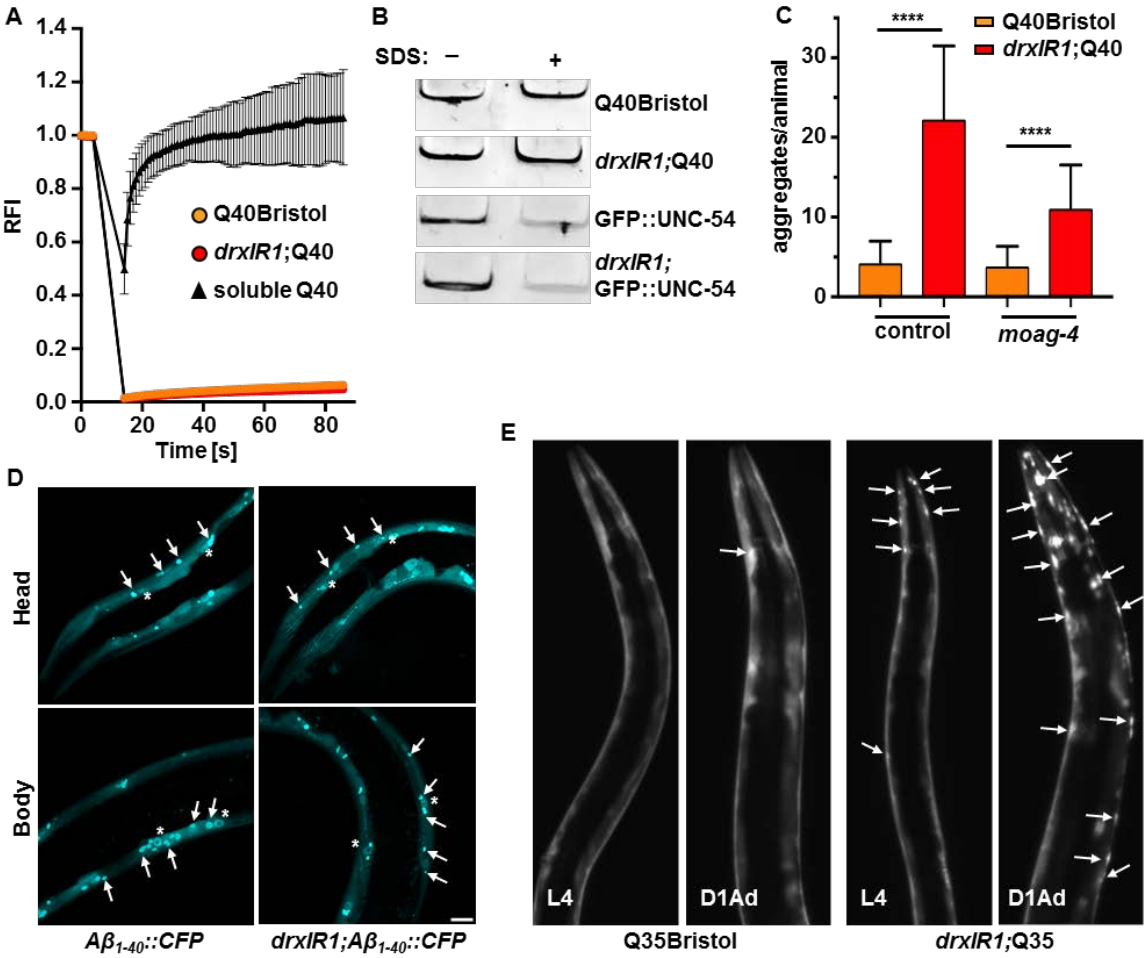

Fig 3. Variants in *drxIR1* interval do not alter the biophysical properties of polyQ aggregates.

(**A**) FRAP analysis of fluorescent polyQ40. The soluble Q40::YFP protein recovered rapidly (**triangles**), while aggregated protein (**circles**) in both Q40Bristol and *drxIR1;*Q40 backgrounds does not recover. Data are mean ± SD. (**B**) PolyQ40 aggregates in *drxIR1*;Q40 remain SDS-resistant. Native extracts containing polyQ aggregates were treated with 5% SDS for 15 minutes and resolved by native PAGE. Aggregated proteins fail to enter the gel, remaining in the wells (shown). Native extracts containing the fibrillar GFP::UNC-54 protein were used as controls. (**C**) The increased aggregation phenotype in animals carrying the *drxlR1* interval does not depend on the amyloid-specific modifier *moag-4*. *moag-4* RNAi decreased the total number of aggregates in both backgrounds (YA animals are shown in Suppl. Fig. 3B), but preserved the increased aggregation in *drxIR1*;Q40 animals relative to Q40Bristol. Data are mean ± SD, three independent experiments. Data were analyzed by ANOVA followed by Bonferroni's multiple comparison test, ****P<0.0001. A total of 38 to 46 mid-L4 animals per condition. (**D**) Aggregation of a different amyloid protein, $A\beta_{1-40}$::CFP, in unaffected by the *drxlR1* locus. Shown are confocal stacks, **arrows** point to aggregates, **asterisks** indicate $A\beta_{1-40}$::CFP accumulating in the nuclei of the muscle cells. Scale bar: 10µm. (**E**) The shorter polyQ expansion (Q35::YFP) exhibits both the increased susceptibility of the head muscle cells and the accelerated overall aggregation in animals

carrying the *drxlR1* interval. Shown are stereo micrographs, **arrows** point to some of the aggregates. **D1Ad**: day 1 adults.

The increased aggregation is specific to polyglutamine expansions

To determine whether the variants responsible for increasing polyQ40 aggregation in *drxIR1*;Q40 animals were acting generically on any amyloid aggregates, we asked if they can modify an aggregation-prone Aβ peptide. We chose the muscle specific $A\beta_{1-40}$::CFP transgene (61) because it exhibits both soluble and aggregated protein early in adulthood, allowing us to detect the potential increase in aggregation. We found that introduction of the *drxIR1* interval did not increase Aβ aggregation (**Fig. 3D**). In contrast, when the *drxIR1* locus was introduced into another polyglutamine model, Q35Bristol, we observed both the overall increase in polyQ35 aggregation and the increased susceptibility of the head muscles (**Fig. 3E**).

These data indicate that the DR1350-derived variants in *drxIR1* background act by a polyglutamine-specific mechanism that is likely distinct from the known aggregation-modifying mechanisms. In addition, the effect on the Q35::YFP and Q40::YFP but not on $A\beta_{1-40}$::CFP transgenic proteins confirms that the novel mechanism acts at the protein level, rather than by modifying the transgene genomic environment, since all three transgenes were made by the same approach.

Increased polyQ40 aggregation in the body-wall muscle cells and increased susceptibility of the head muscles to aggregation are caused by genetically separable mechanisms

Since we were unable to narrow down the candidate genes by identifying affected pathways, and our data pointed to a potentially novel pathway, we turned to an unbiased investigation of genes in the interval. As we previously reported (38), the increased susceptibility of the head muscles to aggregation (RIL2-like phenotype, measured as the ratio of head to body aggregation) behaves as a recessive trait (**Suppl. Table 1, top row**), and is fully suppressed in *drxIR1* heterozygous (*drxIR1/+*;Q40) animals. Thus we asked whether it was caused by a loss-of-function of a gene or genes in the interval, by testing whether it can be rescued in the *drxIR1* homozygotes by introducing a wild-type copy of the interval. We used a free duplication sDp2 that covers the left arm of Chromosome I, through *dpy-5* gene in the center of the Chromosome (41). Introduction of sDP2 into animals homozygous for the *drxIR1* interval and for the known loss-of-function *dpy-5(e61)* allele suppressed both the *dpy* and the RIL2-like head phenotypes to the same extent (**Suppl. Table 2, second row**), indicating that the head-muscles susceptibility

phenotype in *drxIR1* animals is caused by a loss-of-function variant(s), and therefore can potentially be identified by RNAi approach in Q40Bristol animals.

In contrast, the second polyQ phenotype, the increased overall aggregation (as scored in the body-wall muscles alone, excluding the head muscles), was not suppressed in animals heterozygous for the *drxIR1* interval (**Fig. 4A**). Moreover, introduction of the sDP2 duplication, carrying the wild-type (Bristol) copy of this interval, into either Q40Bristol or *drxIR1*;Q40 animals resulted in sharply increased aggregation of polyQ40 in the body-wall muscles, relative to the corresponding strains without the duplication (**Fig. 4A**). This suggests that the phenotype of increased aggregation in the body-wall muscles depends on the dosage of a gene or genes within the boundaries of the modifier interval, and that in *drxIR1*;Q40 animals this gene carries hypermorphic variant(s), mimicking increased gene dosage. Thus, the candidate gene may be identified by RNAi approach in *drxIR1*;Q40 animals.

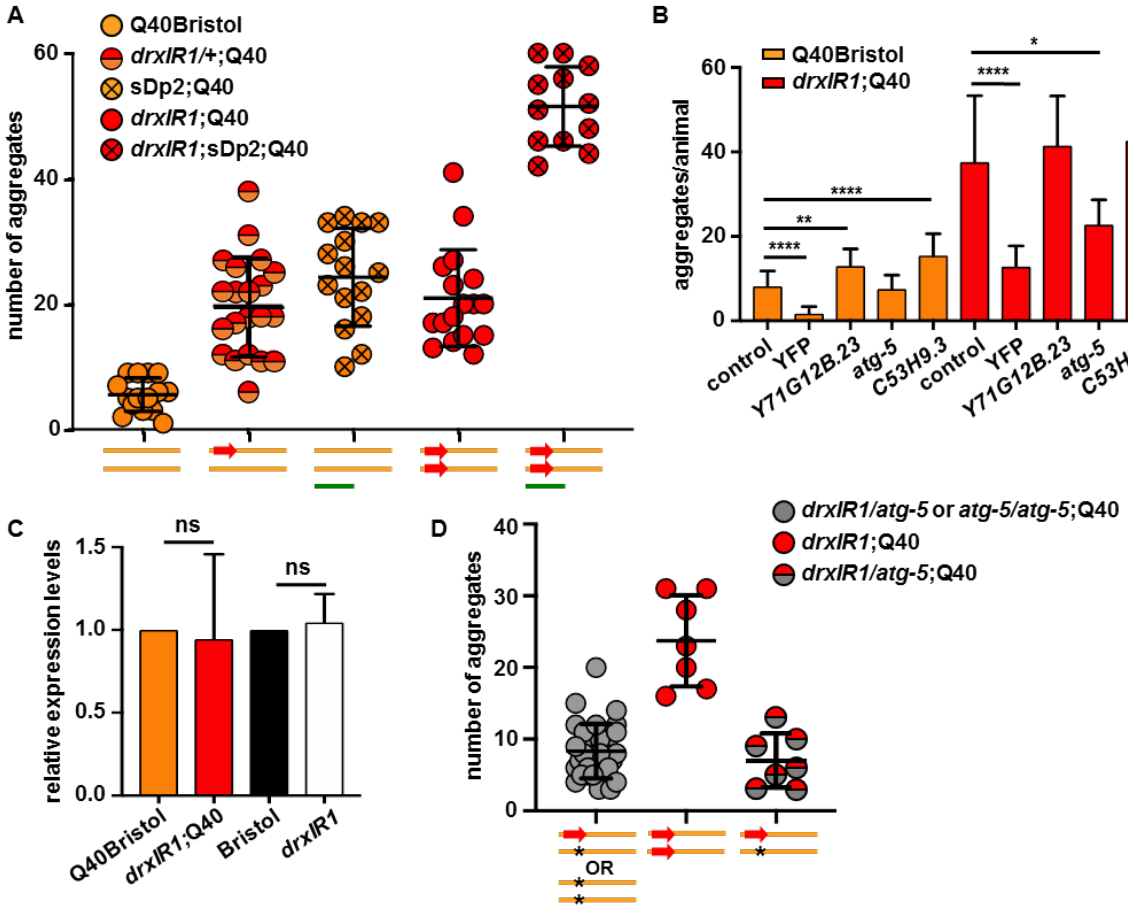

Fig 4. Hypermorphic variants in the autophagy gene *atg-5* are responsible for the increased polyQ aggregation in the body-wall muscles.

(**A**) PolyQ aggregation in the body-wall muscles is sensitive to the dosage of the *drxIR1* interval, with DR1350-derived interval acting as a hypermorph relative to the Bristol-derived interval. Each symbol represents an individual mid-L4 animal; overlaid are means ± SD.

Schematic under the graph represents the genetic composition of Chromosome I: Bristol background (**orange bar**), DR1350-derived *drxlR1* interval (**red arrow**), and the free duplication sDp2 (**green bar**). (**B**) RNAi of three candidate genes affects polyQ40 aggregation. *atg-5* RNAi suppresses the increased polyQ aggregation in the muscle cells of *drxlR1* but not in Q40Bristol animals. RNAi against YFP downregulates expression of Q40::YFP protein. Data are mean ± SD, three independent experiments, 9 to 15 animals per experiment per genotype. Data were analyzed by ANOVA followed by Bonferroni's multiple comparisons test, ****P<0.0001, **P=0.0029, *P=0.0125. (**C**) Relative expression of *atg-5* mRNA is unaffected by the DR1350-derived *drxIR1* interval. Three independent experiments, statistics as in panel B. (**D**) *atg-5(bp484)* loss-of-function allele reverses increased aggregation caused by one copy of the DR1350-derived *drxIR1* interval. Schematic under the graph as in panel A, **star**: *atg-5* mutation. Animals were scored at mid-L4 as in panel A, compare *drxIR1/+*;Q40 animals (red/orange symbols) in panel A with *drxIR1/atg-5*;Q40 animals (red/grey symbols) in panel D. **Grey symbols** represent animals that were assumed (but not confirmed) to be heterozygous for the *drxIR1* interval, because they did not show the RIL2-like phenotype head muscle phenotype and because *atg-5/atg-5* animals exhibit strong developmental delay. Heterozygosity of *drxIR1/atg-5*;Q40 animals (**red/grey symbols**) was confirmed by singling them out and scoring segregation of the RIL2-like phenotype among their progeny. Each symbol represents an individual animals, overlaid are means ± SD.

Autophagy-related gene 5 (ATG-5) is responsible for increased aggregation

To decrease the number of genes that were to be tested by RNAi, we were able to further narrow the large *drxIR1* interval to approximately 326 Kb (ChrI:1,647,221-1,972,719) by additionally backcrossing the *drxIR1*;Q40 animals and using the SNPs in the interval to detect recombination. The smaller 326 Kb interval contained 57 total genes including 25 candidate protein-coding genes with potentially functionally-significant SNPs (based on SnpEff annotations (62), see Methods), with 24 candidate genes remaining after exclusion of *egl-30* (**Suppl. Table 2 and Data File 1**). Each of the candidate genes was knocked down by feeding RNAi in both Q40Bristol and *drxIR1*;Q40 animals, followed by quantification of polyQ aggregation.

None of the RNAi clones affected the increased susceptibility of the head muscles to polyQ aggregation (measured as a ratio of head to body aggregation) in either background. This may potentially indicate that more than one gene in the interval was responsible for the switch in the head muscle susceptibility, or that it depends on SNPs in non-coding RNAs, intergenic regions, or genes with SNPs that were not selected as potentially functionally significant; alternatively, this failure could be due to an inefficient knock-down. On the other hand, RNAi of several genes modified the second phenotype – the overall aggregation of polyQ40 in the body-

wall muscle cells. Decreasing expression of two genes, *Y71G12B.23* and *C53H9.3* caused an increase in the number of aggregates in the Q40Bristol animals, with no change in the *drxIR1*;Q40 animals, while knocking down expression of *atg-5* caused a large decrease in aggregation in the *drxIR1*;Q40 strain, with no effect in the Q40Bristol background (**Fig. 4B**). Because reversal of increased aggregation specifically in *drxIR1*;Q40 animals by RNAi is consistent with our genetic analysis for this phenotype in **Fig. 4A**, which suggested that the causative variant in *drxIR1* background will be hypermorphic, this points to *atg-5* as a candidate gene. In agreement, our genome sequencing of *drxIR1*;Q40 strain uncovered two unique SNPs in the 3'UTR of *atg-5* (**Data File 1)**.

Because a hypermorphic effect can be caused by increased expression of the affected gene or protein, and because the SNPs are localized in the regulatory region of *atg-5*, we first measured *atg-5* transcripts. qPCR data revealed no differences in *atg-5* transcript levels in *drxIR1* or *drxIR1*;Q40 animals compared to their respective Bristol strains (**Fig. 4C**). Thus, we asked whether decreasing the protein expression *via* a targeted deletion of *atg-5* could reverse the increased polyQ aggregation in *drxIR1*;Q40 animals, as expected if the variants were hypermorphic. We used *atg-5(bp484)* allele, which has a mutation in a splice donor site of exon 1 disrupting the protein's expression or function (63, 64). We found that unlike animals that carried one DR1350-derived and one wild-type (Bristol) copy of the interval (*drxIR1/+*;Q40), which we found previously to still exhibit increased aggregation (**Fig. 4A**), *drxIR1* heterozygous animals carrying the *atg-5* mutation in the wild-type interval (*drxIR1/atg-5*;Q40) completely lost the increased aggregation phenotype (**Fig. 4D**). Together, our data suggest that increased levels or activity of ATG-5 protein cause increased polyglutamine aggregation in the body-wall muscle cells.

Activation of autophagy has divergent effects on polyQ aggregation in different tissues

ATG-5 is an ortholog of the autophagic budding yeast protein ATG5, and of human ATG5. ATG-5 contributes to the initiation of autophagy by forming a complex with LGG-3/ATG12 and ATG-16/ATG16L1, which is recruited to the membrane of the elongating phagophore (65-67), and is required for the lipidation of LGG-1/LC3. Thus, upregulation or activation of ATG-5 by the hypermorphic allele could cause either overactivation or an imbalance in autophagy. Interestingly, ATG5 in mammalian cells can also contribute to the progression of apoptosis, independent of its role in autophagy (68).

Although we saw no increase in the number of GFP::LGG-1 puncta in the muscle cells of

drxIR1 animals under basal conditions (**Fig. 2A**), we did observe more puncta in the hypodermal cells, where autophagy is often scored (69). Thus, we asked whether autophagy the muscle cells was different in *drxIR1* and wild-type (Bristol) animals under activation conditions. We used an autophagy inducer drug, ABT-737, that acts as a BH3-mimetic, inhibiting the antagonistic effects of Bcl-2 (CED-9 in worms) on Beclin-1 (BEC-1) and thus relieving the inhibition of autophagy (70). Treatment with 10µM of ABT-737 indeed induced GFP::LGG-1 puncta in the muscle cells of the wild type (Bristol) animals (**Fig. 5A**). Surprisingly, animals carrying the *drxIR1* interval exhibited an increase in punctate appearance of GFP::LGG-1 protein in the body-wall muscle cells already in response to the DMSO control. Although not previously reported to activate autophagy, low concentrations of DMSO have been reported to extend the lifespan of *C. elegans* and decrease the paralysis associated with $A\beta_{1\text{-}42}$ aggregation, when grown in liquid (71, 72). Importantly, ABT-737 resulted in a larger increase in GFP-positive puncta in *drxIR1*;GFP::LGG-1 animals compared to the Bristol background (**Fig. 5A**). These data suggest that *drxIR1* interval increases accumulation of LGG-1/LC31-positive autophagosome structures in response to an activating treatment.

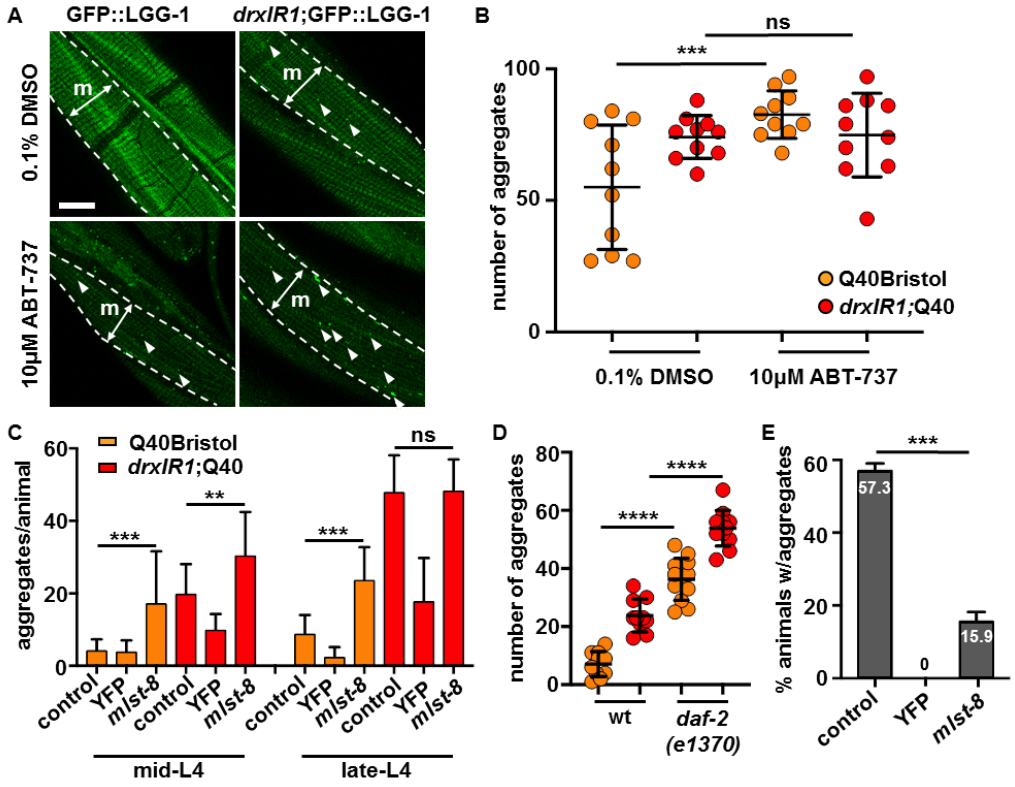

Fig 5. Activation of autophagy has divergent effects on polyQ40 aggregates clearance in different tissues.

(**A**) Animals carrying the *drxIR1* interval accumulate more GFP::LGG-1-positive puncta (**arrowheads**) in the body-wall muscle cells upon treatment with autophagy-activating drug

ABT-737. Animals were treated with 0.1% DMSO (vehicle control) or 10 μM ABT-737 for 24hr. Shown are confocal projections; one muscle quadrant (**m**) is indicated between punctate lines. Scale bar: 10μm. (**B**) Autophagy-activating drug ABT-737 increases polyQ40 aggregation in the body-wall muscle cells in the wild-type background (Q40Bristol). Aggregation was scored in adult animals, 1 day post L4 (see Methods). Aggregation in the *drxIR1*;Q40 animals is already at maximum under these conditions. Each symbol indicates an individual animal; overlaid are means ± SD. Data were analyzed by ANOVA followed by Bonferroni's multiple comparisons test, ***P=0.0006. (**C**) Activation of autophagy with *mlst-8* RNAi increases aggregation in the body-wall muscles of Q40Bristol mid- or late-L4 animals, and of *drxIR1*;Q40 mid-L4 animals. Aggregation in *drxIR1*;Q40 late-L4 animals is already at maximum. Data are mean ± SD, three independent experiments, 9 to 13 animals per experiment per treatment. Control RNAi was *mec-4*. Data were analyzed by ANOVA followed by Bonferroni's multiple comparisons test, ***P=0.0007, **P=0.0082. (**D**) Introduction of the *daf-2(e1370)* allele increases polyQ40 aggregation in the body-wall muscles in both Q40Bristol and *drxIR1*;Q40 animals. Aggregation was scored at mid-L4. Each symbol indicates an individual animal; overlaid are means ± SD. Data were analyzed by ANOVA with Bonferroni's multiple comparisons test, ****P<0.0001. (**E**) Activation of autophagy with *mlst-8* RNAi strongly suppresses polyQ aggregation in the intestinal cells. Percent of animals with Q44::YFP aggregates in the intestine of day 4 adult were scored, as in refs(73, 74), for each indicated RNAi treatment. Control RNAi was *mec-4*. Data are mean ± SD. Data were analyzed by ANOVA followed by Bonferroni's multiple comparisons test, ***P=0.0003.

The larger increase in LGG-1 puncta in *drxIR1*;GFP::LGG-1 animals could indicate that *atg-5* hypermorphic allele causes either a stronger activation of autophagy, or slower lysosomal degradation. Because autophagy is known to promote clearance of polyglutamine aggregates (75), the increased aggregation in *drxIR1* background appeared consistent with slower degradation, while activation of autophagy would have been expected to decrease aggregation (76). To confirm this, we asked whether activation of autophagy with ABT-737 indeed decreased polyQ aggregation in the wild type (Bristol) background. Surprisingly, treatment of Q40Bristol animals with this autophagy activator resulted in a large increase, rather than decrease, of polyQ40 aggregation in the body-wall muscles, with ABT-737-treated animals exhibiting a 44% increase in the number of aggregates (**Fig. 5B**). These data suggest that, counter to expectations, activation of autophagy may enhance polyglutamine aggregation. We did not detect a further increase in aggregation in *drxIR1* background, since the drug treatment protocol dictated scoring aggregates in young adult animals (see materials and methods), when aggregation in *drxIR1*;Q40 is already close to maximal.

Because this effect of autophagy was unexpected, and because the drug treatment may

not be reliable in *C. elegans*, we tested two different genetic approaches known to activate autophagy to confirm these findings. Each of the two approaches activates autophagy *via* mechanisms distinct from that of ABT-737. First common approach is inactivation of mTOR (77). In *C. elegans*, inactivation of LET-363/mTOR indeed activates autophagy, as shown by increase in GFP::LGG-1 puncta (78). However, inactivation of LET-363 also causes larval arrest (79), which itself will affect polyQ aggregation. To overcome this, we targeted mTOR interacting protein MLST-8/mLST8, which is required for the kinase activity of mTOR (80), but can be downregulated in *C. elegans* without causing larval arrest (81). RNAi knock-down of *mlst-8* resulted in a 1.6-fold increase in polyQ40 aggregation in Q40Bristol animals (**Fig. 5C**, late-L4). Similar to the results of the drug treatment, *mlst-8* RNAi had no significant effect in *drxIR1*;Q40 animals. We asked whether the apparent lack of effect on the *drxIR1*;Q40 animals was indeed due to the already high aggregate numbers at this developmental stage, by repeating the RNAi in younger animals, and observed an even stronger, 3-fold, increase in polyQ40 aggregation in Q40Bristol animals, and a 1.5-fold increase in *drxIR1*;Q40 animals (**Fig. 5C**, mid-L4).

As a second genetic approach, we tested the effect of decreased activity of insulin/IGF-like signaling pathway, since reduction of function of the sole *C. elegans* orthologue of insulin/IGF receptor, DAF-2, is known to cause activation of autophagy, including in the body-wall muscle cells (52, 82). Introduction of the hypomorphic *daf-2(e1370)* allele caused a 5.1-fold increase in aggregates in the Q40Bristol background, and 2.3-fold further increase in *drxIR1*;Q40 animals (**Fig. 5D).** The increase in polyQ aggregation in *daf-2(e1370)* background is consistent with previous reports (83). Together, these pharmacological, RNAi, and genetic data suggest that aggregation of polyQ40 in the body-wall muscle cells is paradoxically increased by activation of autophagy.

Previous studies indicate that autophagy levels, both basally and in response to a trigger, can be different in different *C. elegans* and mammalian tissues (51, 84). Intriguingly, in these reports, mouse slow-twitching muscles showed nearly no basal autophagy and only low to moderate induction in response to starvation (84), and *C. elegans* body-wall muscle cells also showed low basal autophagy compared to other tissues (51, 52), consistent with our observation of the low numbers of LGG-1-positive puncta in the muscle cells in **Fig. 2C**. Thus, we asked whether activation of autophagy may have a different effect on polyQ aggregation in muscles than in a different tissue. In addition to the muscle-expressed polyQs, the neuronal and intestinal fluorescent polyQ models have been described in *C. elegans* (73, 85). Since aggregation of the

moderate polyQ40 expansions in neurons is only detectable by FRAP, we chose to examine the intestinal polyQ44 model. We found that unlike in the muscle-expressed polyQ model, activation of autophagy *via* RNAi knock-down of *mlst-8* resulted in a large (3.5-fold) decrease in the percentage of animals exhibiting polyglutamine aggregation in intestine (**Fig. 5E**). Thus, depending on the tissue, activation of autophagy can either clear polyglutamine aggregates or cause their accumulation.

Discussion

Using natural genetic variation, we identified an unexpected divergence in how activation of autophagy in different tissues impacts the behavior of aggregation-prone polyglutamine expansions. It is broadly appreciated that autophagy can be both protective and detrimental to cells and organisms (86). For example, ER stress-induced autophagy is protective in cancer cells but contributes to apoptosis in non-transformed cells (87), while starvation-triggered autophagy in *C. elegans* pharyngeal muscle can switch from protective to pro-death, depending on its level of activation (50). However, with respect to the clearance of misfolded aggregated proteins, activation of autophagy is generally considered to be a positive, protective response (88, 89). Therefore, activation of autophagy has been thought of as a nearly universal therapeutic approach to neurodegenerative diseases caused by protein aggregation (90). While we did not test the neuronal polyQ models, the divergence in how polyQ expansions in intestinal and muscle cells respond to activation of autophagy suggests that interplay between autophagy and protein aggregation depends on the cellular context. We find that both the natural variants in *atg-5*, and the more traditional genetic and pharmacological ways of activating autophagy, increased rather than decreased polyQ aggregation in the muscle cells of *C. elegans*. This represents a striking departure from the current paradigm. On the other hand, polyQ aggregation in the intestinal cells, as expected, was decreased by the same treatment. Considering the significant involvement of skeletal muscle and non-neuronal tissues in HD and other polyglutamine diseases, including the induction of the muscle catabolic phenotype and muscle wasting (91-95), a more nuanced understanding of integration of autophagy with cellular physiology is needed.

The use of natural variation was instrumental in uncovering this unexpected cell-specific effect of autophagy on protein aggregation. The DR1350-derived variants that we identified as being responsible for the increased aggregation of polyQ40 in the muscle cells are in the regulatory 3'UTR region of the *atg-5* gene. Our genetic analysis points to the gain of expression as the mechanism of *atg-5* variants. Based on the ability of one additional copy of the wild-type,

Bristol-derived *atg-5* to mimic the effect of these natural variants (**Fig. 4A**), and because deletion of one copy of *atg-5* reverses the effect of the variants in the remaining copy (**Fig. 4D**), we estimate that the variants increase the expression of ATG-5 protein by less than 2-fold. Strikingly, introduction of one additional Bristol-derived copy of *atg-5* into the animals already carrying two DR1350-derived hypermorphic alleles, increases the polyQ aggregation even further, to about 6-fold above normal. This indicates a quantitative relationship between the levels of ATG-5 protein and increased polyQ aggregation in the muscle. Although we are currently unable to directly modulate autophagy in *C. elegans* in a graded manner, the ability of three distinct methods of activating autophagy to mimic the effect of the variants argues that the increase in ATG-5 affects the polyQ aggregation by increasing autophagy, rather than for example by causing stoichiometric imbalance and autophagy inhibition (76), or coupling to apoptosis pathway (68). The precise mechanistic basis of this quantitative relationship will need to be investigated further.

One important aspect of our findings is the cryptic nature of the modifier variants in *atg-5*. Cryptic variation typically does not cause phenotypic changes on its own, but becomes phenotypically "exposed" when challenged with a stressful environment, thus contributing to disease susceptibility (96-98). Polyglutamine expansions may mimic cellular stress, for example by destabilizing the folding environment (37) or disrupting transcriptional control (99). Indeed, the *atg-5* variants identified here as modifiers are derived from a phenotypically normal wild strain DR1350, and we did not detect significant alterations in the basal autophagy in the muscles of *drxIR1* animals unless they were challenged with the aggregation-prone polyQ40, or with autophagy-activating drug ABT-737.

In addition to being exposed by stress, the phenotypic expression of cryptic modifier variants may reflect their more direct interactions with the disease-causing mutation. For example, in humans, analysis of HD modifier loci on Chromosomes 8 and 15 showed that these variants influence certain clinical readouts in subjects with expanded polyQ tracts, prior to the appearance of disease symptoms, while they have no major effects in control individuals without expansions (18). The suspected culprit for the modifying effect of the Chromosome 15 locus, the DNA endo/exonuclease FAN1, may be changing the disease phenotypes or age of onset by directly affecting the stability of the polyQ-encoding repeat in somatic tissues (18, 100).

Interestingly, the HD disease progression study (18) suggested that the modifiers could have distinct modifying effects in different cell populations. In our study, the cryptic nature of the *atg-5* variants allowed detection of the unusual cell-specificity in autophagy - aggregation

relationship, because non-cryptic genetic variants that ectopically activate autophagy already under basal conditions have additional strong phenotypes that can mask the effects of activated autophagy on polyQ aggregation. For example, loss of function of *C. elegans* mTOR leads to larval arrest (79); hypomorphic mutations in insulin/IGF signaling pathway, in addition to activating autophagy, trigger numerous other developmental, stress responsive, and metabolic pathways (101-103) that can have their own effects on the aggregation-prone protein; and even non-genetic means such as activation of autophagy by nutrient deprivation are accompanied by the metabolic and protein expression changes (104) that can mask the more specific effect on the polyQ behavior. Natural variation may thus indeed identify the candidate modifier pathways and mechanistic relationships in aggregation diseases that are distinct from those identified by the traditional approaches.

The reasons the muscle cells are differentially sensitive to autophagy with respect to protein aggregation, or why this is not true for other aggregation-prone proteins, are not yet known. The selectivity of aggregation effects of autophagy towards the polyglutamine expansions would argue against a global dysregulation of protein homeostasis in the muscle cells of *drxIR1*animals, which is supported by our data. It is possible however, that ectopic activation of autophagy disrupts select proteostasis processes that impinge on the polyQ aggregation or clearance in these cells. Another possibility is that autophagic degradation of polyQ expansions requires a specific "signal" or adaptor, which may be competed away during generic increase in autophagy in the muscle cells, but remains sufficient in the intestine. The polyQ-expanded huntingtin protein (Htt) indeed requires specific adaptors, such as Tollip, to be cleared by autophagy (105), although whether this is also true for polyQ expansions outside the Htt context is not clear. Yet another possibility is that polyQ expansions themselves interfere with autophagy. For example, polyQ-expanded Htt have been suggested to interfere with the delivery of cargoes to autophagic vacuoles (106), and shown to co-aggregate with the autophagy adaptor Tollip, potentially disrupting other functions of this multi-tasking protein (105). If so, the low basal levels of autophagy may render the proteostasis of the muscle cells to be more sensitive to the polyQ expansions.

Muscle cells may also have a different regulation of or dependence on autophagy because autophagy of the muscle is an adaptive response of many metazoans to starvation (107). While basal autophagy is important for muscle maintenance, not only deficiency in autophagy but also its over-activation can lead to muscle atrophy (108-110). Indeed, in *C. elegans*, body-wall muscles in young animals have low basal levels of autophagy relative to other tissues (51, 52),

while in mice, the slow-twitching (soleus) muscles exhibited little induction of autophagy after 24 hours of starvation, as defined by the autophagosome counts, distinct from the fast-twitching (extensor digitorum longus) muscles that had significant induction (84). Moreover, the distribution of autophagosomes was different between the fast- and slow-twitching muscle types, supporting the idea of differential autophagy regulation in different cells or tissues.

In addition to the traditional mouse models, the genetic model systems such as worm, fly and yeast, in which natural variation can be readily combined with modeling the gain-of-function mutations by transgenesis, offer new opportunities to identify the cryptic modifier pathways for neurodegeneration and protein misfolding and aggregation (10, 111-115). Examples of this approach include a recent study in *C. elegans* that showed that the ability of α-synuclein to cause transcriptional and phenotypic changes is substantially modified by the genetic background (40), and a study using a Drosophila Genetic Reference Panel (116), that uncovered an unexpected role of heparin sulfate protein modifications in modifying the toxic effects of the misfolded mutant of human insulin, a cause of permanent neonatal diabetes (117). The important feature of the cryptic modifier pathways that can be identified by these approaches is that they harbor natural variants shaped by selection, and thus will pinpoint the naturally plastic potential genes and networks (14), amenable to pharmacological manipulation without negative effects on the organism.

Materials and Methods

Nematode strains and growth conditions

Nematodes were grown at 20°C on nematode growth medium (NGM) plates, seeded with *E. coli* OP50 (118). Animals were synchronized by picking gastrula stage embryos onto fresh plates, unless otherwise noted.

The following stains were obtained from *Caenorhabditis* Genetics Center (CGC): AM141 [*rmIs333*(p*unc-54*::Q40::YFP)], AM140 [*rmIs132*(p*unc-54*::Q35::YFP) I], CF1038 [*daf-16(mu86)* I], TJ356 [*zIs356(*p*daf-16::daf-16a/b*::GFP;*pRF4(rol-6(su1006)*) IV], PS3551 [*hsf-1(sy441)* I], DA2123 [*adIs2122*(p*lgg-1*::GFP::*lgg-1 + rol-6(su1006)*)], KR1108 [*unc-11(e47) dpy-5(e61)* I], KR292 [*him-1(h55) dpy-5(e61) unc-13(e450)* I; sDp2 (I;f)], MT1434 [*egl-30(n686)* I], and CB1370 [*daf-2(e1370)* III]. TGF205 [*xzEx3*(p*unc-54*::UbG76V::Dendra2)] was made by crossing out *glp-1(e2141)* from AGD1033.

The AS408 [p*unc-54*::GFP::UNC-54], AM583 [*rmIs249*(p*let-858::hsf-1;*p*myo-2::*GFP*)*], AM738 [*rmIs297*(p*vha-6*::Q44::YFP;*rol-6(su1006)*)], and AM930 [*rmIs335*(p*unc-54*::Aβ(1-

40)::CFP)] strains were kindly provided by the Morimoto lab, and the HZ1732 [*atg-5(bp484)* I;*him-5*] strain by the Colón-Ramos lab. The Q40DR1350 and recombinant inbred lines (RILs) 2, 12, 12(2) and 15 were described in (38).

The *drxIR1*(I, DR1350>Bristol) locus and/or the Q40 locus were introduced by genetic crosses into the following strains: TGF134 [*drxIR1*;*rmIs333*(p*unc-54*::Q40::YFP)], TGF130 [*drxIR1*;p*unc-54*::GFP::UNC-54], TGF353 [*drxIR1*;*adIs2122*(p*lgg-1*::GFP::*lgg-1 + rol-6(su1006)*)], TGF208 [*xzEx3*(p*unc-54*::UbG76V::Dendra2);*rmIs333*(p*unc-54*::Q40::YFP)], TGF207 [*drxIR1*;*xzEx3*(p*unc-54*::UbG76V::Dendra2);*rmIs333*(p*unc-54*::Q40::YFP)], TGF088 [*daf-16(mu86)* I; *rmIs333*(p*unc-54*::Q40::YFP)], TGF188 [*drxIR1*;*daf-16(mu86)* I;*rmIs333*(p*unc-54*::Q40::YFP)], TGF086 [*zIs356(*p*daf-16::daf-16a/b*::GFP;*pRF4(rol-6(su1006)*) IV;*rmIs333*(p*unc-54*::Q40::YFP)], TGF190 [*drxIR1*;*zIs356(*p*daf-16::daf-16a/b*::GFP;*pRF4(rol-6(su1006)*) IV;*rmIs333*(p*unc-54*::Q40::YFP)], TGF187 [*hsf-1(sy441)* I;*rmIs333*(p*unc-54*::Q40::YFP)], TGF170 [*drxIR1*;*hsf-1(sy441)* I;*rmIs333*(p*unc-54*::Q40::YFP)], TGF036 [*rmIs249*(p*let-858::hsf-1;*p*myo-2::*GFP);*rmIs333*(p*unc-54*::Q40::YFP)], TGF189 [*drxIR1*; *rmIs249*(p*let-858::hsf-1;*p*myo-2::*GFP);*rmIs333*(p*unc-54*::Q40::YFP)], TGF203 [*drxIR1*;*rmIs335*(p*unc-54*::Aβ(1-40)::CFP)], TGF342 [*drxIR1*;*rmIs132*(p*unc-54*::Q35::YFP) I], TGF261 [*rmIs333*(p*unc-54*::Q40::YFP);*him-1(h55) dpy-5(e61) unc-13(e450)* I; sDp2 (I;f)] TGF275 [*drxIR1*;*rmIs333*(p*unc-54*::Q40::YFP);*him-1(h55) dpy-5(e61) unc-13(e450)* I; sDp2 (I;f)], TGF089 [*daf-2(e1370)* III;*rmIs333*(p*unc-54*::Q40::YFP)]; TGF127 [*drxIR1;daf-2(e1370)* III;*rmIs333*(p*unc-54*::Q40::YFP)].

The *drxIR1*;Q40 strain was made by the following scheme: Q40Bristol males were mated to RIL2 hermaphrodites, and 5-10 F1 hermaphrodite progeny, identified by the lack of RIL2-like increased head aggregation phenotype, were picked onto fresh plates. F2 generation was examined for the expected 1:3 segregation of the increased head aggregation phenotype, and 7-10 F2 hermaphrodites with this phenotype were further mated with Q40Bristol males. This mating-selection cycle was repeated 23 times. The resulting strain was named *drxIR1;*Q40.

The introduction of *drxIR1* locus by genetic crosses was confirmed by detecting the presence of the SNP 5 (WBVar00016276) (**Suppl. Fig. 1**): a 743bp fragment containing the variant was amplified using the *drxIR1* primers (**Suppl. Table 3**), at an annealing temperature of 60°C, to produce an amplicon of 743bp, and the PCR product was digested with SalI. The SalI site is present in the Bristol background, producing 432bp and 311bp products after the digest, but is absent in the DR1350 background.

Genome sequencing

Genomic DNA from *drxIR1*;Q40 and Q40Bristol was extracted from flash frozen pellets of a mixed populations, using phenol:chloroform (Sigma, USA). DNA was sequenced using the NextSeq 500 System (Illumina, USA) at the Wistar Institute (Philadelphia PA, USA). Sequencing data was analyzed using the Galaxy (119) CloudMap pipeline as described in (42), and WS220 genome assembly. The CloudMap SnpEff tool was utilized to annotate the genetic variants and predict their functional effects on genes and proteins (62). SNPs with the following annotations were considered as potentially functionally-significant: non-synonymous coding, start gained or lost, stop gained or lost, splice site donor/acceptor, frameshift, and 5' or 3' UTR.

Quantification of polyQ40 aggregation

Aggregation was scored by counting fluorescent foci in images collected from animals immobilized with 20 mM NaN_3, using a Leica M205FA stereoscope with a digital camera (Hamamatsu Orca R2). For synchronization, 15-20 well-fed L4 animals from non-crowded plates were transferred to new plates, gastrula stage embryos were picked 2-3 days later, and hatched animals were allowed to develop for specified time or to specified developmental stage. Aggregation was scored in late-L4 animals, unless otherwise indicated. The developmental larval stage was confirmed based on the germline development, or by days since L4 (for older adults). For data expressed as means, the number of animals for each data point is indicated in the figure legends.

Microscopy

For confocal images, animals were immobilized on 2% agar pads with 20 mM NaN_3 and imaged with Zeiss LSM700 microscope at Cell Imaging Center, Drexel University. Z-stacks were acquired at 0.4 µm intervals as 12-bit images, using 63x 1.4NA objective, and analyzed with ImageJ. For the quantification of autophagic vesicles, Z-stacks were collapsed as maximum intensity projections, the muscle cells were outlined, and the GFP::LGG-1-positive puncta within the outlined cells were counted. 30 to 40 cells from 8 to 10 L4 animals were analyzed per genotype. To compare GFP::UNC-54 protein levels, GFP fluorescence was measured within the same size area (~9μm^2) in the center of each analyzed muscle cell, over the myofilaments. 16-20 cells from 4-5 animals per genotype were measured. An identical size area measured away from the myofilaments was used for background subtraction.

Fluorescent recovery after photobleaching (FRAP) was performed on day 2 adults (for

aggregated Q40) and L4 larvae (for soluble Q40) animals, as in (85), using the Zeiss LSM700 confocal microscope. Photobleaching was performed with 488 nm laser, by 100 iterations at 100% laser power. Imaging during recovery was at 0.2% power. Relative fluorescence intensity (RFI) was determined with the following equation: RFI = $(T_t/C_t)/(T_0/C_0)$, with T_0 representing the total intensity of the region of interest before photobleaching and T_t the intensity in the same are at any time after. We normalized against an unbleached area in the same cell, where C_0 is a control area before bleaching and C_t represents any time after bleaching (85). 7-18 aggregates from 3 animals each were measured per strain for aggregated Q40, and 5 cells from 2 animals each were measured per strain for the soluble Q40 controls.

For stereo images, animals were immobilized on NGM plates in a drop of 20 mM NaN_3. Imaging was performed using a Leica M205FA stereo microscope with an Orca R2 digital camera (Hamamatsu). The magnification and the intensity of fluorescent sources (Chroma PhotoFluor 2) were kept constant within experiments. UbG76V::Dendra2 animals were imaged with a narrow-bandpass CFP filter (Chroma), to avoid the spectral overlap with the Q40::YFP protein.

Native protein extracts

To prepare native protein extracts, synchronized embryos were prepared by hypochlorite treatments and larvae were collected once they reached the L3 stage. The worm pellets were mechanically disrupted and lysed in 0.5% Triton-X 100 buffer as described in (39). For SDS solubility, native protein extracts were incubated in 5% SDS for 15 min at room temperature prior to running on a 5% continuous native-PAGE, at 25 mg of total protein per lane. Gels were imaged on a Typhoon FLA7000 scanner (General Electric, USA) with ImageQuant TL software to quantify YFP fluorescence. All experiments were performed three times.

qPCR

~50µl pellets of L4 stage worms were flash frozen in liquid nitrogen and RNA extraction was performed using TRIzol (Life Technologies, USA) and chloroform (Sigma, USA) reagents. The samples were treated with DNase (DNA-*free*, Life Technologies, USA) to remove any genomic DNA, and iScript cDNA synthesis kit (Bio-Rad, USA) was used to reverse transcribe 1-2 µg of RNA per sample. The expression of selected genes was measured using iTaq Universal SYBR Green Supermix (company) and the ViiA detector (Applied Biosystems). Each biological replicate was run in triplicate, and data analyzed using the ΔΔCT method (120). Three

biological replicates were used to assess statistical significance. Tubulin (*tbg-1*) was used as the internal control, as it was stable between the *drxIR1* and the Bristol strains. *tbg-1* primers were obtained from (121). Primer sequences are listed in **Suppl. Table 3**.

RNAi experiments and constructs

For RNAi experiments, NGM plates containing 100 µg/ml ampicillin and 0.4 mM IPTG were seeded with control (L4440 empty vector, unless otherwise noted) or experimental overnight RNAi bacterial cultures and incubated at room temperature for 2 days prior to plating worms. Nematodes were cultured on the RNAi plates from gastrula stage embryos for two generations. RNAi strains were from the Ahringer library (J. Ahringer, University of Cambridge, Cambridge, U.K.), except for those corresponding to *mab-20, Y71G12B.18, Y71G12B.33, Y71G12B.23, Y71G12B.35, drag-1, Y71G12B.31, ubc-3, tln-1, Y71G12B.25, pghm-1, C53H9.3, tag-96, tub-2, Y51F10.4, and spe-48*; these were made by cloning a unique 0.8 to 1.2 Kb fragment from each gene into the L4440 plasmid and transforming into the *E. coli* strain HT115. Primer sequences are listed in **Suppl. Table 4**. All experiments were repeated three times, the total (combined) number of animals is indicated in figure legends.

ABT-737 treatment

20-40 gastrula stage embryos were grown on OP50 bacteria for two days at 20°C, nematodes collected, washed, and exposed to either 0.1% DMSO (Sigma, USA) as solvent control, or 10 µM ABT-737 (ApexBio, Taiwan). Earlier exposure to ABT-737 resulted in larval arrest. Animals were incubated in the drug solution with shaking for 24 hours, pipetted onto plates, and either scored for aggregation or imaged.

Statistical analyses

ANOVA and *t*-test analyses were performed with Prism software (GraphPad, USA), using α value of 0.5. ANOVA was followed by Bonferroni's multiple comparisons post-test. All p-values and significance levels are indicated in the figures and figure legends.

Acknowledgements

We thank the Colón-Ramos lab at Yale School of Medicine and the Morimoto lab at Northwestern University for contributing worm strains. Some strains were provided by the *Caenorhabditis* Genetics Center (CGC) at the University of Minnesota, which is funded by NIH

Office of Research Infrastructure Programs (P40OD010440). We would like to thank Anna Lysenko for experimental assistance.

Supplemental Files

Suppl. Fig 1. Schematic of the *drxlR1*interval and SNPs used for mapping.
Red: the 1.4Mb genomic region on Chromosome I containing the DR1350-derived intervals in the RIL2-derived *drxlR1*;Q40 strain and the four remaining high aggregation RILs (RIL12, RIL12(2), RIL18 and RIL15); **orange**: the Bristol background. **Punctate lines** delineate the narrowed 326 Kb interval containing the candidate genes tested by RNAi. **Diamonds**: SNPs used to confirm the presence of the interval; SNP 6b (ChrI:1,972,719 (WBVar00017376)) is Bristol-derived in *drxIR1*;Q40 and RIL15 animals. **L**ocations of *egl-30*, *moag-4* and the incompatibility locus *zeel-1/peel-1*are also indicated. The coordinates here correspond to the WormBase release WS270 (122).

Suppl. Fig 2. Cumulative distribution of unique SNPs across remaining Chromosomes.
Chromosomes II through X in the *drxlR1*;Q40 strain accumulated up to 160 unique SNPs each. Shown are SNPs remaining after subtraction of the variants present in the parental Q40Bristol strain and the known Hawaii SNPs.

Suppl. Fig 3. Controls for basal proteostasis effects of the *drxIR1* locus
(**A**) The UbG76V::Dendra2 proteasome reporter is sensitive to decreased proteasome levels. Knockdown of a proteasome subunit *rpn-6.1*, via RNAi, increased the average intensity of the Dendra2 compared to control treatment. Images were taken and quantified as in Fig. 2D. Data are mean ± SD. Data were analyzed by unpaired *t*-test, two-tailed, **P*=0.0244. (**B**) Stereomicrographs of **young adult** animals after treatment with control or *moag-4* RNAi. *moag-4* RNAi decreased aggregation in both backgrounds, but preserved the increased aggregation *drxIR1*;Q40 animals relative to Q40Bristol.

Suppl. Table 1. Loss-of-function analysis for the RIL2-like head aggregation phenotype.
sDP2 free duplication covers most of the left arm of Chromosome I, extending through *dpy-5* marker but not through *unc-13*. *drxIR1*;Q40 animals were crossed with KR292 [*him-1(h55);dpy-*

*5(e61);unc-13(e450)*I; sDp2(I;f)], F1 progeny that either did (based on segregation of *unc* non-*dpy* phenotype among their progeny) or did not inherit the sDp2 duplication were singled, and their F2 progeny scored for the increased ratio of head to body aggregation (RIL2-like) and the dumpy phenotypes. The RIL2-like phenotype behaved genetically as did the known loss-of-function *dpy-5(e61)* allele.

Suppl. Table 2. Candidate genes tested by RNAi.

24 candidate genes present in the target 326 Kb of *drxIR1* interval (between SNPs 5 and 6b (**Suppl. Fig. 1**)) are indicated in color. Genes were defined as candidates based on the SnpEff annotations (see Methods and **Data File 1**). *egl-30* was excluded based on genetic crosses. Genes in **purple** were targeted by clones from the Ahringer RNAi library. RNAi targeting constructs for genes in **red** were prepared in this work.

Suppl. Table 3. Primers used for genotyping the *drxIR1* locus and for qPCR analysis of *atg-5* expression.

Suppl. Table 4. Primers used for generating RNAi clones.

Data File 1. List of genes with potentially significant SNPs generated by the SnpEff tool.

The nucleotide positions correspond to the N2(Bristol) genome assembly from WormBase release WS220 (122), available in the UCSC Genome Browser as ce10. The presence of human orthologs is according to (123).

References

1. Ross CA & Poirier MA (2004) Protein aggregation and neurodegenerative disease. *Nature medicine* 10 Suppl:S10-17.
2. David DC, *et al.* (2010) Widespread protein aggregation as an inherent part of aging in C. elegans. *PLoS biology* 8(8):e1000450.
3. Carrell RW & Lomas DA (1997) Conformational disease. *Lancet* 350(9071):134-138.
4. Bucciantini M, *et al.* (2002) Inherent toxicity of aggregates implies a common mechanism for protein misfolding diseases. *Nature* 416(6880):507-511.
5. Zoghbi HY & Orr HT (2000) Glutamine repeats and neurodegeneration. *Annual review of neuroscience* 23:217-247.
6. Chen S, Ferrone FA, & Wetzel R (2002) Huntington's disease age-of-onset linked to polyglutamine aggregation nucleation. *Proceedings of the National Academy of Sciences of the United States of America* 99(18):11884-11889.
7. Shao J & Diamond MI (2007) Polyglutamine diseases: emerging concepts in pathogenesis and therapy. *Human molecular genetics* 16 Spec No. 2:R115-123.
8. Fu H, Hardy J, & Duff KE (2018) Selective vulnerability in neurodegenerative diseases. *Nature neuroscience* 21(10):1350-1358.
9. Brichta L & Greengard P (2014) Molecular determinants of selective dopaminergic vulnerability in Parkinson's disease: an update. *Frontiers in neuroanatomy* 8:152.
10. Wang YA, Kammenga JE, & Harvey SC (2017) Genetic variation in neurodegenerative diseases and its accessibility in the model organism Caenorhabditis elegans. *Human genomics* 11(1):12.
11. Figueroa KP, *et al.* (2017) Genetic analysis of age at onset variation in spinocerebellar ataxia type 2. *Neurology. Genetics* 3(3):e155.
12. Wexler NS, *et al.* (2004) Venezuelan kindreds reveal that genetic and environmental factors modulate Huntington's disease age of onset. *Proceedings of the National Academy of Sciences of the United States of America* 101(10):3498-3503.
13. Gusella JF & MacDonald ME (2009) Huntington's disease: the case for genetic modifiers. *Genome medicine* 1(8):80.
14. Hamilton BA & Yu BD (2012) Modifier genes and the plasticity of genetic networks in mice. *PLoS genetics* 8(4):e1002644.
15. Li JL, *et al.* (2003) A genome scan for modifiers of age at onset in Huntington disease: The HD MAPS study. *American journal of human genetics* 73(3):682-687.
16. Li JL, *et al.* (2006) Genome-wide significance for a modifier of age at neurological onset in Huntington's disease at 6q23-24: the HD MAPS study. *BMC medical genetics* 7:71.
17. Gayan J, *et al.* (2008) Genomewide linkage scan reveals novel loci modifying age of onset of Huntington's disease in the Venezuelan HD kindreds. *Genetic epidemiology* 32(5):445-453.
18. Long JD, *et al.* (2018) Genetic Modification of Huntington Disease Acts Early in the Prediagnosis Phase. *American journal of human genetics* 103(3):349-357.
19. Genetic Modifiers of Huntington's Disease C (2015) Identification of Genetic Factors that Modify Clinical Onset of Huntington's Disease. *Cell* 162(3):516-526.
20. Lee JM, *et al.* (2017) A modifier of Huntington's disease onset at the MLH1 locus. *Human molecular genetics* 26(19):3859-3867.
21. Chao MJ, *et al.* (2018) Population-specific genetic modification of Huntington's disease in Venezuela. *PLoS genetics* 14(5):e1007274.

22. Haider NB, Ikeda A, Naggert JK, & Nishina PM (2002) Genetic modifiers of vision and hearing. *Human molecular genetics* 11(10):1195-1206.
23. Marsh JL, Lukacsovich T, & Thompson LM (2009) Animal models of polyglutamine diseases and therapeutic approaches. *The Journal of biological chemistry* 284(12):7431-7435.
24. Jackson GR, *et al.* (1998) Polyglutamine-expanded human huntingtin transgenes induce degeneration of Drosophila photoreceptor neurons. *Neuron* 21(3):633-642.
25. Warrick JM, *et al.* (1998) Expanded polyglutamine protein forms nuclear inclusions and causes neural degeneration in Drosophila. *Cell* 93(6):939-949.
26. Faber PW, Alter JR, MacDonald ME, & Hart AC (1999) Polyglutamine-mediated dysfunction and apoptotic death of a Caenorhabditis elegans sensory neuron. *Proceedings of the National Academy of Sciences of the United States of America* 96(1):179-184.
27. Marsh JL, *et al.* (2000) Expanded polyglutamine peptides alone are intrinsically cytotoxic and cause neurodegeneration in Drosophila. *Human molecular genetics* 9(1):13-25.
28. Kazemi-Esfarjani P & Benzer S (2000) Genetic suppression of polyglutamine toxicity in Drosophila. *Science* 287(5459):1837-1840.
29. Parker JA, *et al.* (2001) Expanded polyglutamines in Caenorhabditis elegans cause axonal abnormalities and severe dysfunction of PLM mechanosensory neurons without cell death. *Proceedings of the National Academy of Sciences of the United States of America* 98(23):13318-13323.
30. Morley JF, Brignull HR, Weyers JJ, & Morimoto RI (2002) The threshold for polyglutamine-expansion protein aggregation and cellular toxicity is dynamic and influenced by aging in Caenorhabditis elegans. *Proceedings of the National Academy of Sciences of the United States of America* 99(16):10417-10422.
31. Satyal SH, *et al.* (2000) Polyglutamine aggregates alter protein folding homeostasis in Caenorhabditis elegans. *Proceedings of the National Academy of Sciences of the United States of America* 97(11):5750-5755.
32. Christie NT, Lee AL, Fay HG, Gray AA, & Kikis EA (2014) Novel polyglutamine model uncouples proteotoxicity from aging. *PloS one* 9(5):e96835.
33. Fardghassemi Y, Tauffenberger A, Gosselin S, & Parker JA (2017) Rescue of ATXN3 neuronal toxicity in Caenorhabditiselegans by chemical modification of endoplasmic reticulum stress. *Disease models & mechanisms* 10(12):1465-1480.
34. Teixeira-Castro A, *et al.* (2011) Neuron-specific proteotoxicity of mutant ataxin-3 in C. elegans: rescue by the DAF-16 and HSF-1 pathways. *Human molecular genetics* 20(15):2996-3009.
35. Kikis EA, Gidalevitz T, & Morimoto RI (2010) Protein homeostasis in models of aging and age-related conformational disease. *Advances in experimental medicine and biology* 694:138-159.
36. Hsu AL, Murphy CT, & Kenyon C (2003) Regulation of aging and age-related disease by DAF-16 and heat-shock factor. *Science* 300(5622):1142-1145.
37. Gidalevitz T, Ben-Zvi A, Ho KH, Brignull HR, & Morimoto RI (2006) Progressive disruption of cellular protein folding in models of polyglutamine diseases. *Science* 311(5766):1471-1474.
38. Gidalevitz T, Wang N, Deravaj T, Alexander-Floyd J, & Morimoto RI (2013) Natural genetic variation determines susceptibility to aggregation or toxicity in a C. elegans model for polyglutamine disease. *BMC biology* 11:100.
39. Gidalevitz T, Krupinski T, Garcia S, & Morimoto RI (2009) Destabilizing protein polymorphisms in the genetic background direct phenotypic expression of mutant SOD1 toxicity. *PLoS genetics* 5(3):e1000399.

40. Wang YA, *et al.* (2019) Genetic background modifies phenotypic and transcriptional responses in a C. elegans model of alpha-synuclein toxicity. *BMC genomics* 20(1):232.
41. Rose AM, Baillie DL, & Curran J (1984) Meiotic pairing behavior of two free duplications of linkage group I in Caenorhabditis elegans. *Molecular & general genetics : MGG* 195(1-2):52-56.
42. Minevich G, Park DS, Blankenberg D, Poole RJ, & Hobert O (2012) CloudMap: a cloud-based pipeline for analysis of mutant genome sequences. *Genetics* 192(4):1249-1269.
43. Koch R, van Luenen HG, van der Horst M, Thijssen KL, & Plasterk RH (2000) Single nucleotide polymorphisms in wild isolates of Caenorhabditis elegans. *Genome research* 10(11):1690-1696.
44. Sarin S, *et al.* (2010) Analysis of multiple ethyl methanesulfonate-mutagenized Caenorhabditis elegans strains by whole-genome sequencing. *Genetics* 185(2):417-430.
45. Seidel HS, Rockman MV, & Kruglyak L (2008) Widespread genetic incompatibility in C. elegans maintained by balancing selection. *Science* 319(5863):589-594.
46. Sassi HE, Renihan S, Spence AM, & Cooperstock RL (2005) Gene CATCHR--gene cloning and tagging for Caenorhabditis elegans using yeast homologous recombination: a novel approach for the analysis of gene expression. *Nucleic Acids Res* 33(18):e163.
47. Bejsovec A & Anderson P (1988) Myosin heavy-chain mutations that disrupt Caenorhabditis elegans thick filament assembly. *Genes & development* 2(10):1307-1317.
48. Barral JM, Hutagalung AH, Brinker A, Hartl FU, & Epstein HF (2002) Role of the myosin assembly protein UNC-45 as a molecular chaperone for myosin. *Science* 295(5555):669-671.
49. Landsverk ML, *et al.* (2007) The UNC-45 chaperone mediates sarcomere assembly through myosin degradation in Caenorhabditis elegans. *The Journal of cell biology* 177(2):205-210.
50. Kang C, You YJ, & Avery L (2007) Dual roles of autophagy in the survival of Caenorhabditis elegans during starvation. *Genes & development* 21(17):2161-2171.
51. Chapin HC, Okada M, Merz AJ, & Miller DL (2015) Tissue-specific autophagy responses to aging and stress in C. elegans. *Aging* 7(6):419-434.
52. Chang JT, Kumsta C, Hellman AB, Adams LM, & Hansen M (2017) Spatiotemporal regulation of autophagy during Caenorhabditis elegans aging. *eLife* 6.
53. Vilchez D, *et al.* (2012) RPN-6 determines C. elegans longevity under proteotoxic stress conditions. *Nature* 489(7415):263-268.
54. Lin K, Dorman JB, Rodan A, & Kenyon C (1997) daf-16: An HNF-3/forkhead family member that can function to double the life-span of Caenorhabditis elegans. *Science* 278(5341):1319-1322.
55. Henderson ST & Johnson TE (2001) daf-16 integrates developmental and environmental inputs to mediate aging in the nematode Caenorhabditis elegans. *Current biology : CB* 11(24):1975-1980.
56. Hajdu-Cronin YM, Chen WJ, & Sternberg PW (2004) The L-type cyclin CYL-1 and the heat-shock-factor HSF-1 are required for heat-shock-induced protein expression in Caenorhabditis elegans. *Genetics* 168(4):1937-1949.
57. Ben-Zvi A, Miller EA, & Morimoto RI (2009) Collapse of proteostasis represents an early molecular event in Caenorhabditis elegans aging. *Proceedings of the National Academy of Sciences of the United States of America* 106(35):14914-14919.
58. Scherzinger E, *et al.* (1997) Huntingtin-encoded polyglutamine expansions form amyloid-like protein aggregates in vitro and in vivo. *Cell* 90(3):549-558.
59. Falsone SF, *et al.* (2012) SERF protein is a direct modifier of amyloid fiber assembly. *Cell reports* 2(2):358-371.

60. van Ham TJ, *et al.* (2010) Identification of MOAG-4/SERF as a regulator of age-related proteotoxicity. *Cell* 142(4):601-612.
61. Roth DM, *et al.* (2014) Modulation of the maladaptive stress response to manage diseases of protein folding. *PLoS biology* 12(11):e1001998.
62. Cingolani P, *et al.* (2012) A program for annotating and predicting the effects of single nucleotide polymorphisms, SnpEff: SNPs in the genome of Drosophila melanogaster strain w1118; iso-2; iso-3. *Fly* 6(2):80-92.
63. Zhang H, *et al.* (2013) The two C. elegans ATG-16 homologs have partially redundant functions in the basal autophagy pathway. *Autophagy* 9(12):1965-1974.
64. Stavoe AK, Hill SE, Hall DH, & Colon-Ramos DA (2016) KIF1A/UNC-104 Transports ATG-9 to Regulate Neurodevelopment and Autophagy at Synapses. *Developmental cell* 38(2):171-185.
65. Mizushima N, *et al.* (1998) A protein conjugation system essential for autophagy. *Nature* 395(6700):395-398.
66. Mizushima N, Noda T, & Ohsumi Y (1999) Apg16p is required for the function of the Apg12p-Apg5p conjugate in the yeast autophagy pathway. *The EMBO journal* 18(14):3888-3896.
67. Melendez A & Levine B (2009) Autophagy in C. elegans. *WormBook : the online review of C. elegans biology*:1-26.
68. Yousefi S, *et al.* (2006) Calpain-mediated cleavage of Atg5 switches autophagy to apoptosis. *Nature cell biology* 8(10):1124-1132.
69. Zhang H, *et al.* (2015) Guidelines for monitoring autophagy in Caenorhabditis elegans. *Autophagy* 11(1):9-27.
70. Maiuri MC, *et al.* (2007) Functional and physical interaction between Bcl-X(L) and a BH3-like domain in Beclin-1. *The EMBO journal* 26(10):2527-2539.
71. Wang X, Wang X, Li L, & Wang D (2010) Lifespan extension in Caenorhabditis elegans by DMSO is dependent on sir-2.1 and daf-16. *Biochemical and biophysical research communications* 400(4):613-618.
72. Frankowski H, *et al.* (2013) Dimethyl sulfoxide and dimethyl formamide increase lifespan of C. elegans in liquid. *Mechanisms of ageing and development* 134(3-4):69-78.
73. Mohri-Shiomi A & Garsin DA (2008) Insulin signaling and the heat shock response modulate protein homeostasis in the Caenorhabditis elegans intestine during infection. *The Journal of biological chemistry* 283(1):194-201.
74. Prahlad V & Morimoto RI (2011) Neuronal circuitry regulates the response of Caenorhabditis elegans to misfolded proteins. *Proceedings of the National Academy of Sciences of the United States of America* 108(34):14204-14209.
75. Ravikumar B, Duden R, & Rubinsztein DC (2002) Aggregate-prone proteins with polyglutamine and polyalanine expansions are degraded by autophagy. *Human molecular genetics* 11(9):1107-1117.
76. Jia K, Hart AC, & Levine B (2007) Autophagy genes protect against disease caused by polyglutamine expansion proteins in Caenorhabditis elegans. *Autophagy* 3(1):21-25.
77. Saxton RA & Sabatini DM (2017) mTOR Signaling in Growth, Metabolism, and Disease. *Cell* 168(6):960-976.
78. Hansen M, *et al.* (2008) A role for autophagy in the extension of lifespan by dietary restriction in C. elegans. *PLoS genetics* 4(2):e24.
79. Long X, *et al.* (2002) TOR deficiency in C. elegans causes developmental arrest and intestinal atrophy by inhibition of mRNA translation. *Current biology : CB* 12(17):1448-1461.

80. Kim DH, *et al.* (2003) GbetaL, a positive regulator of the rapamycin-sensitive pathway required for the nutrient-sensitive interaction between raptor and mTOR. *Molecular cell* 11(4):895-904.
81. Jones KT, Greer ER, Pearce D, & Ashrafi K (2009) Rictor/TORC2 regulates Caenorhabditis elegans fat storage, body size, and development through sgk-1. *PLoS biology* 7(3):e60.
82. Melendez A, *et al.* (2003) Autophagy genes are essential for dauer development and life-span extension in C. elegans. *Science* 301(5638):1387-1391.
83. Cohen E, Bieschke J, Perciavalle RM, Kelly JW, & Dillin A (2006) Opposing activities protect against age-onset proteotoxicity. *Science* 313(5793):1604-1610.
84. Mizushima N, Yamamoto A, Matsui M, Yoshimori T, & Ohsumi Y (2004) In vivo analysis of autophagy in response to nutrient starvation using transgenic mice expressing a fluorescent autophagosome marker. *Molecular biology of the cell* 15(3):1101-1111.
85. Brignull HR, Moore FE, Tang SJ, & Morimoto RI (2006) Polyglutamine proteins at the pathogenic threshold display neuron-specific aggregation in a pan-neuronal Caenorhabditis elegans model. *The Journal of neuroscience : the official journal of the Society for Neuroscience* 26(29):7597-7606.
86. Nikoletopoulou V, Markaki M, Palikaras K, & Tavernarakis N (2013) Crosstalk between apoptosis, necrosis and autophagy. *Biochimica et biophysica acta* 1833(12):3448-3459.
87. Ding WX, *et al.* (2007) Differential effects of endoplasmic reticulum stress-induced autophagy on cell survival. *The Journal of biological chemistry* 282(7):4702-4710.
88. Nixon RA (2013) The role of autophagy in neurodegenerative disease. *Nature medicine* 19(8):983-997.
89. Ciechanover A & Kwon YT (2015) Degradation of misfolded proteins in neurodegenerative diseases: therapeutic targets and strategies. *Experimental & molecular medicine* 47:e147.
90. Menzies FM, *et al.* (2017) Autophagy and Neurodegeneration: Pathogenic Mechanisms and Therapeutic Opportunities. *Neuron* 93(5):1015-1034.
91. Zielonka D, Piotrowska I, Marcinkowski JT, & Mielcarek M (2014) Skeletal muscle pathology in Huntington's disease. *Frontiers in physiology* 5:380.
92. Huang S, *et al.* (2015) Large Polyglutamine Repeats Cause Muscle Degeneration in SCA17 Mice. *Cell reports* 13(1):196-208.
93. Luthi-Carter R, *et al.* (2002) Dysregulation of gene expression in the R6/2 model of polyglutamine disease: parallel changes in muscle and brain. *Human molecular genetics* 11(17):1911-1926.
94. Moffitt H, McPhail GD, Woodman B, Hobbs C, & Bates GP (2009) Formation of polyglutamine inclusions in a wide range of non-CNS tissues in the HdhQ150 knock-in mouse model of Huntington's disease. *PloS one* 4(11):e8025.
95. She P, *et al.* (2011) Molecular characterization of skeletal muscle atrophy in the R6/2 mouse model of Huntington's disease. *Am J Physiol Endocrinol Metab* 301(1):E49-61.
96. Rutherford SL & Lindquist S (1998) Hsp90 as a capacitor for morphological evolution. *Nature* 396(6709):336-342.
97. Gibson G (2009) Decanalization and the origin of complex disease. *Nature reviews. Genetics* 10(2):134-140.
98. Paaby AB & Rockman MV (2014) Cryptic genetic variation: evolution's hidden substrate. *Nature reviews. Genetics* 15(4):247-258.
99. Luthi-Carter R, *et al.* (2002) Polyglutamine and transcription: gene expression changes shared by DRPLA and Huntington's disease mouse models reveal context-independent effects. *Human molecular genetics* 11(17):1927-1937.

100. Goold R, *et al.* (2019) FAN1 modifies Huntington's disease progression by stabilizing the expanded HTT CAG repeat. *Human molecular genetics* 28(4):650-661.
101. Walker DW, McColl G, Jenkins NL, Harris J, & Lithgow GJ (2000) Evolution of lifespan in C. elegans. *Nature* 405(6784):296-297.
102. Jenkins NL, McColl G, & Lithgow GJ (2004) Fitness cost of extended lifespan in Caenorhabditis elegans. *Proceedings. Biological sciences* 271(1556):2523-2526.
103. Chen J, *et al.* (2007) A demographic analysis of the fitness cost of extended longevity in Caenorhabditis elegans. *The journals of gerontology. Series A, Biological sciences and medical sciences* 62(2):126-135.
104. Altman BJ & Rathmell JC (2012) Metabolic stress in autophagy and cell death pathways. *Cold Spring Harbor perspectives in biology* 4(9):a008763.
105. Lu K, Psakhye I, & Jentsch S (2014) Autophagic clearance of polyQ proteins mediated by ubiquitin-Atg8 adaptors of the conserved CUET protein family. *Cell* 158(3):549-563.
106. Martinez-Vicente M, *et al.* (2010) Cargo recognition failure is responsible for inefficient autophagy in Huntington's disease. *Nature neuroscience* 13(5):567-576.
107. Schiaffino S, Dyar KA, Ciciliot S, Blaauw B, & Sandri M (2013) Mechanisms regulating skeletal muscle growth and atrophy. *The FEBS journal* 280(17):4294-4314.
108. Mammucari C, *et al.* (2007) FoxO3 controls autophagy in skeletal muscle in vivo. *Cell metabolism* 6(6):458-471.
109. Zhao J, *et al.* (2007) FoxO3 coordinately activates protein degradation by the autophagic/lysosomal and proteasomal pathways in atrophying muscle cells. *Cell metabolism* 6(6):472-483.
110. Masiero E, *et al.* (2009) Autophagy is required to maintain muscle mass. *Cell metabolism* 10(6):507-515.
111. Heiman-Patterson TD, *et al.* (2011) Effect of genetic background on phenotype variability in transgenic mouse models of amyotrophic lateral sclerosis: a window of opportunity in the search for genetic modifiers. *Amyotrophic lateral sclerosis : official publication of the World Federation of Neurology Research Group on Motor Neuron Diseases* 12(2):79-86.
112. Peters TW, *et al.* (2018) Natural Genetic Variation in Yeast Reveals That NEDD4 Is a Conserved Modifier of Mutant Polyglutamine Aggregation. *G3* 8(11):3421-3431.
113. Lloret A, *et al.* (2006) Genetic background modifies nuclear mutant huntingtin accumulation and HD CAG repeat instability in Huntington's disease knock-in mice. *Human molecular genetics* 15(12):2015-2024.
114. Van Raamsdonk JM, *et al.* (2007) Phenotypic abnormalities in the YAC128 mouse model of Huntington disease are penetrant on multiple genetic backgrounds and modulated by strain. *Neurobiol Dis* 26(1):189-200.
115. Chow CY, Wolfner MF, & Clark AG (2013) Using natural variation in Drosophila to discover previously unknown endoplasmic reticulum stress genes. *Proceedings of the National Academy of Sciences of the United States of America* 110(22):9013-9018.
116. Mackay TF, *et al.* (2012) The Drosophila melanogaster Genetic Reference Panel. *Nature* 482(7384):173-178.
117. He BZ, *et al.* (2014) Effect of genetic variation in a Drosophila model of diabetes-associated misfolded human proinsulin. *Genetics* 196(2):557-567.
118. Brenner S (1974) The genetics of Caenorhabditis elegans. *Genetics* 77(1):71-94.
119. Afgan E, *et al.* (2016) The Galaxy platform for accessible, reproducible and collaborative biomedical analyses: 2016 update. *Nucleic Acids Res* 44(W1):W3-W10.
120. Livak KJ & Schmittgen TD (2001) Analysis of relative gene expression data using real-time quantitative PCR and the 2(-Delta Delta C(T)) Method. *Methods* 25(4):402-408.

121. Lascarez-Lagunas LI, Silva-Garcia CG, Dinkova TD, & Navarro RE (2014) LIN-35/Rb causes starvation-induced germ cell apoptosis via CED-9/Bcl2 downregulation in Caenorhabditis elegans. *Mol Cell Biol* 34(13):2499-2516.
122. Lee RYN, *et al.* (2018) WormBase 2017: molting into a new stage. *Nucleic Acids Res* 46(D1):D869-D874.
123. Shaye DD & Greenwald I (2011) OrthoList: a compendium of C. elegans genes with human orthologs. *PloS one* 6(5):e20085.

Supplemental Figure 1

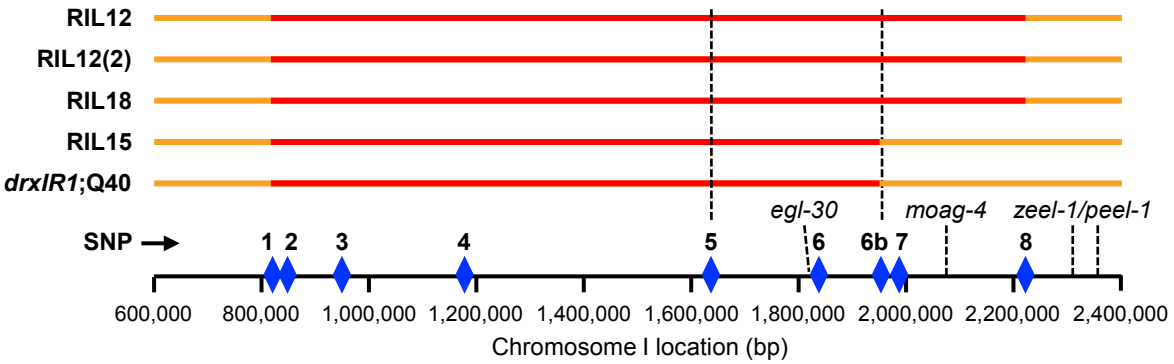

SNP	Variation name	Location (bp)
1	WBVar00004591	832,671
2	WBVar01529903	846,351
3	WBVar01529977	944,150
4	WBVar00014396	1,176,473
5	WBVar00016276	1,647,221
6	WBVar00017051	1,850,249
6b	WBVar00017376	1,972,719
7	WBVar00017401	1,981,603
8	WBVar00023136	2,222,271

Supplemental Figure 2

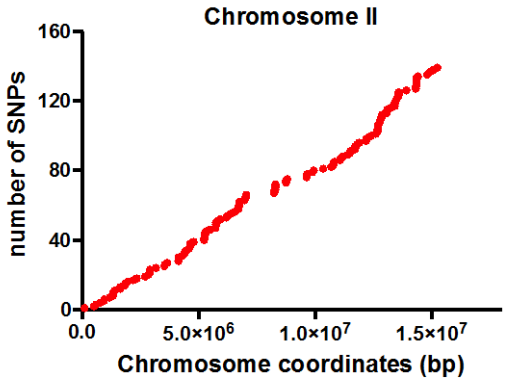

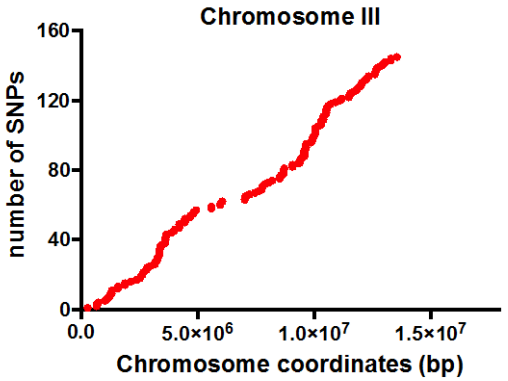

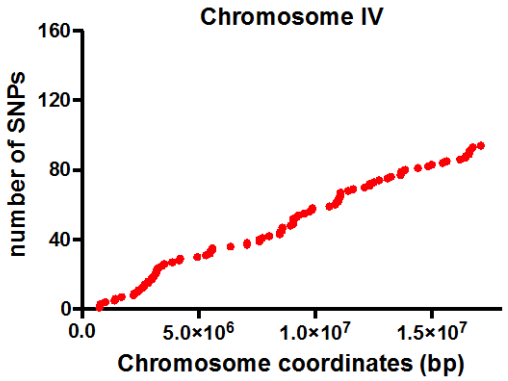

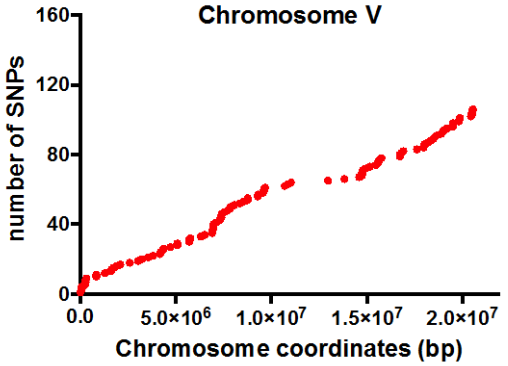

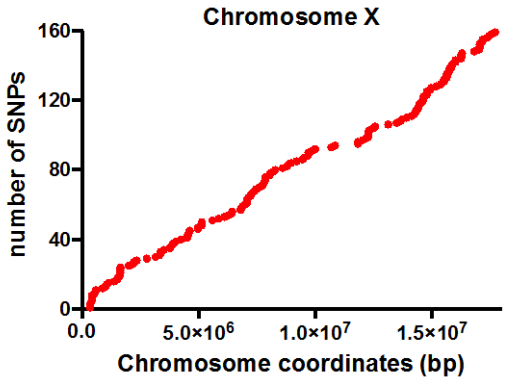

Supplemental Figure 3

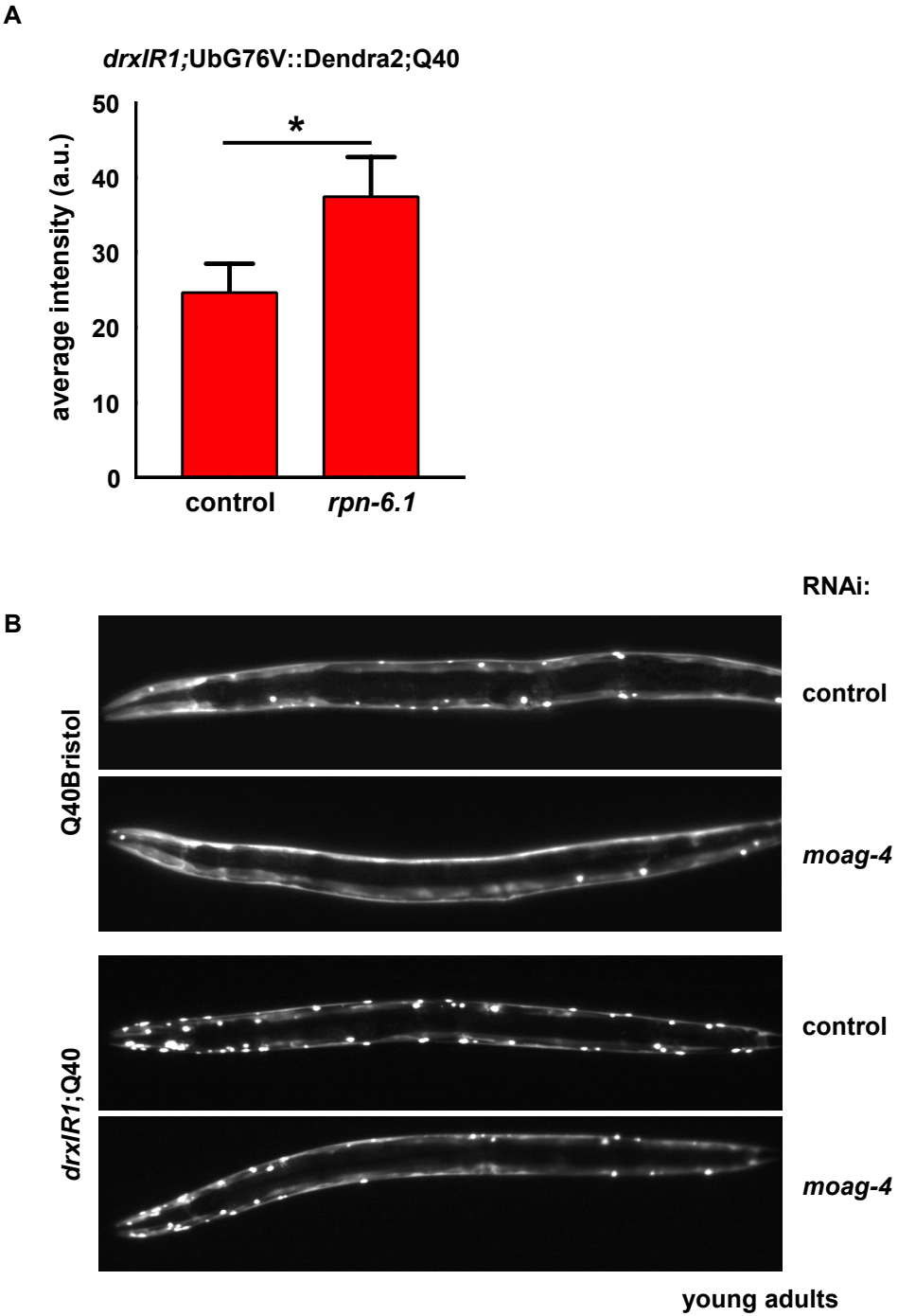

Suppl. Table 1 Loss of function analysis for the increased susceptibility of head muscles to aggregation

F1 animals that *did not* inherit sDp2

# of F1 animals	# of F2 animals scored	# RIL2-like F2 animals	# *dpy* F2 animals	% RIL2-like F2 animals	% *dpy* F2 animals
22	4533	1041	1109	23	24.5

F1 animals that *did* inherit sDp2

# of F1 animals	# of F2 animals scored	# of RIL2-like F2 animals	# of *dpy* F2 animals	%RIL2-like F2 animals	% *dpy* F2 animals
5	707	91	91	12.8	12.8

Suppl. Table 2 Genes located in the 350Kb interval on the left arm of Chromosome I of *drxIR1* animals		
Gene	**Candidate**	**Function/homology/phenotype**
mab-20	+	Semaphorin-2A ortholog; is required for proper epidermal morphogenesis and axon guidance
Y71G12B.18	+	
Y71G12B.33	+	
Y71G12B.17	+	An ortholog of human PITPNB and PITPNA; may have phospholipid transporter activity
Y71G12B.23	+	An ortholog of human MMD and MMD2; may have heme-copper terminal oxidase activity
Y71G12B.35	+	
drag-1	+	A membrane associated protein that functions as a co-receptor in the the Sma/Mab pathway
Y71G12B.31	+	An ortholog of human PTPN7; may have protein tyrosine phosphatase activity
ubc-3	+	E2 ubiquitin-conjugating enzyme
atg-5	+	An ortholog of the autophagic budding yeast protein Atg5p, and of human ATG5
tln-1	+	Talin; a cytoskeleton protein
mppa-1	+	Mitochondrial processing peptidase alpha
lin-65	+	Acts with B class SynMuv genes to repress vulval induction, and is required for fertility. Component of the mitochondrial unfolded protein response
Y71G12B.25	+	An ortholog of human MFSD10
Y71G12B.5	+	
pghm-1	+	Peptidylglycine alpha-hydroxylating monooxygenase
chaf-2	+	Chromatin assembly factor
C53H9.3	+	
egl-30	-	An ortholog of the heterotrimeric G protein alpha subunit Gq; affects viability, locomotion, egg laying, synaptic transmission, and pharyngeal pumping
tag-96	+	A galactokinase that is a member of the GHMP family of kinases
tub-2	+	Tubby-related
Y71G12A.4	+	An ortholog of human ABHD17A and ABHD17C
trpp-10	+	Transport protein particle
Y51F10.4	+	An ortholog of human SLC38A10
spe-48	+	Spermatogenesis defective

Suppl. Table 3 Primers used for genotyping the *drxIR1* locus and for qPCR analysis of *atg-5* expression	
Primer name	**Primer sequence 5'-3'**
drxIR1 fwd.	AAGCCCCGCCGAGTTAAAACCG
drxIR1 rev.	TGGCGACCGAGTGTAGCATCGTG
atg-5 fwd.	CTGGCGGAACTCACGGAG
atg-5 rev.	CGCTTGATCGTAGATCAC
tbg-1 fwd.	CCTGTTGTCGATCCAAATGA
tbg-1 rev.	AACCCGAGAAGCAGTTGAAA

Suppl. Table 4 Primers used for generating RNAi clones

Primer name	Primer sequence 5'-3'
mab-20_HindIII Up	GACGAAGCTTAACTCGGCCACCTATTGAAC
mab-20_NcoI Down	AGTACCATGGAGCAACTGAGAATTGGGAGAC
Y71G12B.18_HindIII Up	GACGAAGCTTGGTAGCGGATGACTGATGTTAG
Y71G12B.18_NcoI Down	ACTTCCATGGAGCTCCTTTACAAACAGGTAGG
Y71G12B.33_NcoI fwd.	AGTACCATGGACGCTTGCCATTCGAAATAAAC
Y71G12B.33_HindIII rev.	TCATAAGCTTCATGCCTCCTCCCATTCATC
Y71G12B.23_HindIII Up	ACTGAAGCTTGATCGGTATAGGACCCACAATTC
Y71G12B.23_NcoI Down	GACTCCATGGGCCGCAATGAACAGGTAAATG
Y71G12B.35_NcoI fwd.	TAGTCCATGGTTGAGTCGAAGGAGCCAAAG
Y71G12B.35_HindIII rev.	TACGAAGCTTTCAAACGGAGCAAATTGAGAAAG
drag-1_HindIII Up	CGTCAAGCTTCTGGAACAGAATAAGTTG
drag-1_NcoI Down	AGCACCATGGCCCATCACATCGTGTCGT
Y71G12B.31_NcoI fwd.	TACTCCATGGCTACTTCTTCTGATGGTAGTTCCTC
Y71G12B.31_HindIII rev.	TACTAAGCCTTCCGTACTGGTGTGTTCATCTG
ubc-3_NcoI fwd.	TACTCCATGGCAGGTGGAAGAGTCGAAGAAAG
ubc-3_HindIII rev.	TACTAAGCTTCGTCATAGTCACACCCGAAATC
tln-1_AB_SalI Up	GCATGTCGACCGTCTCGAACAAGACTGTACTC
tln-1_AB_BglII Down	ACTGAGATCTAGTAGAGCGCGTTTGTATGG
Y71G12B.25_NcoI fwd.	ACTACCATGGCAAGGCAATTTGAGTGTTGGAG
Y71G12B.25_HindIII rev.	TACTAAGCTTTCAATGGTCCAATGGCTCAC
pghm-1_NcoI fwd.	TACTCCATGGAAACAGGAACCCGATGAGAC
pghm-1_HindIII rev.	ATGCAAGCTTGGCTTCACAAACAGATCAACAG
C53H9.3_NcoI fwd.	ATCTCCATGGCAATCCCTTAATTCTTTCCAGA
C53H9.3_HindIII rev.	ATCTAAGCTTCTTGATCCTTACAACGGGTAG
M01D7.4_BglII fwd. (tag-96 fwd.)	TACTAGATCTTCGCCTCAAAGAAATTCAAACC
M01D7.4_SalI rev. (tag-96 rev.)	TGATGTCGACTGCGATGACTCTCGTTCATTAG

Suppl. Table 4 (continued)

Primer name	Primer sequence 5'-3'
Y71G12A.3_NcoI fwd. (tub-2 fwd.)	ATCACCATGGGTTTGTTAAGCACTGCCCTAT
Y71G12A.3_HindIII rev. (tub-2 rev.)	TACTAAGCTTTGGCTACTGAAGCGCTAGTG
Y51F10.4_BglII fwd.	TACTAGATCTAGGAGAGGCAGCATCAGAAG
Y51F10.4_SalI rev.	TACTGTCGACGCTTAAAGCATTTCTGGCAAC
Y51F10.10_NcoI fwd. (spe-48 fwd.)	TACTCCATGGCGTTCAGTAGACACAAAGGAAGAC
Y51F10.10_HindIII rev. (spe-48 rev.)	TACTAAGCTTGATGAAACGTTGCCGTTCTTG

Data File 1

# Chr	Position	Reference	Change	Type	Homoz	Quality	Coverage	Gene_name	Bio_type	Effect	old/new AA	Old/New codon	Codon Degen	Human orthologs
I	1647223	C	G	SNP	Hom	80.72	3	mab-20	Semaphorin	NON_SYNONYMOUS_CODING	V/L	Gtc/Ctc	0	+
I	1648246	T	C	SNP	Hom	404.04	11	mab-20		NON_SYNONYMOUS_CODING	I/V	Atc/Gtc	0	
I	1649294	A	C	SNP	Hom	174.42	7	mab-20		UTR_3_PRIME: 41 bases from CDS				
I	1649298	C	T	SNP	Hom	214.39	8	mab-20		UTR_3_PRIME: 37 bases from CDS				
I	1649399	A	G	SNP	Hom	77.6	3	mab-20		NON_SYNONYMOUS_CODING	F/S	tTt/tCt	0	
I	1653522	C	A	SNP	Hom	486.38	13	Y71G12B.18	protein_coding	NON_SYNONYMOUS_CODING	H/Q	caC/caA	1	
I	1660980	A	T	SNP	Hom	446.38	12	Y71G12B.33	protein_coding	NON_SYNONYMOUS_CODING	L/M	Ttg/Atg	1	
I	1667646	T	C	SNP	Hom	443.35	12	Y71G12B.17	protein_coding	UTR_5_PRIME: 84 bases from TSS				
I	1670189	*		INS	Hom	124.21	8	Y71G12B.23	protein_coding	UTR_3_PRIME: 21 bases from CDS				+
I	1673156	C	A	SNP	Hom	348.73	11	Y71G12B.35	protein_coding	NON_SYNONYMOUS_CODING	G/V	gGa/gTa	0	
I	1680477	G	A	SNP	Hom	420.86	12	drag-1	Sma/Mab regulator	UTR_5_PRIME: 268 bases from TSS				+
I	1682968	T	C	SNP	Hom	324.04	9	drag-1		NON_SYNONYMOUS_CODING	Y/H	Tat/Cat	0	+
I	1687806	C	T	SNP	Hom	287.08	8	Y71G12B.31	protein_coding	NON_SYNONYMOUS_CODING	R/K	aGa/aAa	0	
I	1698160	C	T	SNP	Hom	247.11	7	ubc-3	E2	UTR_5_PRIME: 193 bases from TSS				+
I	1701041	*		INS	Hom	406.03	15	ubc-3		UTR_3_PRIME: 252 bases from CDS				
I	1715498	G	T	SNP	Hom	324.04	9	**atg-5**	autophagy	UTR_3_PRIME: 101 bases from CDS				+
I	1715525	*		DEL	Hom	268.22	11	**atg-5**		UTR_3_PRIME: 128 bases from CDS				
I	1731010	A	T	SNP	Hom	117.15	4	tln-1, unc-35	talin	NON_SYNONYMOUS_CODING	N/I	aAc/aTc	0	+
I	1740691	*		INS	Hom	197.16	8	mppa-1	Mito Processing Peptidase Alpha	UTR_3_PRIME: 74 bases from CDS				+
I	1763076	G	T	SNP	Hom	195.35	6	lin-65	SynMuvB proline rich	NON_SYNONYMOUS_CODING	A/S	Gct/Tct	0	
I	1766320	*	+C	INS	Hom	356.8	10	lin-65		UTR_3_PRIME: 289 bases from CDS				
I	1771464	*		DEL	Hom	141.44	7	Y71G12B.25	protein_coding	UTR_3_PRIME: 80 bases from CDS				
I	1771511	*		INS	Hom	244.19	14	Y71G12B.25		UTR_3_PRIME: 33 bases from CDS				
I	1801557	C	A	SNP	Hom	142.91	6	Y71G12B.5	protein_coding	NON_SYNONYMOUS_CODING	P/T	Cct/Act	0	
I	1801727	A	G	SNP	Hom	415.92	12	Y71G12B.5		NON_SYNONYMOUS_CODING	S/G	Agt/Ggt	0	
I	1802798	A	G	SNP	Hom	183.84	7	Y71G12B.5		NON_SYNONYMOUS_CODING	I/V	Att/Gtt	0	
I	1803484	A	G	SNP	Hom	322.47	12	Y71G12B.5		NON_SYNONYMOUS_CODING	I/M	atA/atG	2	
I	1803485	A	G	SNP	Hom	322.47	12	Y71G12B.5		NON_SYNONYMOUS_CODING	M/V	Atg/Gtg	0	
I	1803997	G	T	SNP	Hom	272.24	8	Y71G12B.5		NON_SYNONYMOUS_CODING	R/L	cGg/cTg	0	

I	1804164	A	G	SNP	Hom	438.38	12	Y71G12B.5		NON_SYNONYMOUS_CODING	T/A	Acc/Gcc	0	
I	1811285	G	A	SNP	Hom	285.65	8	pghm-1	extented lifespan	NON_SYNONYMOUS_CODING	V/I	Gtc/Atc	0	
I	1823449	C	A	SNP	Hom	445.64	12	chaf-2	chromatin assembly	UTR_5_PRIME: 7 bases from TSS				+
I	1825924	*		DEL	Hom	347.6	11	Y71G12B.1		UTR_3_PRIME: 17 bases from CDS				+
I	1832531	G	A	SNP	Hom	401.01	11	C53H9.3	protein_coding	UTR_5_PRIME: 51 bases from TSS				
I	1841231	C	T	SNP	Hom	155.25	6	egl-30	G protein alpha	UTR_3_PRIME: 341 bases from CDS				+
I	1841245	T	C	SNP	Hom	194.5	7	egl-30	subunit	UTR_3_PRIME: 355 bases from CDS				
I	1846453	T	C	SNP	Hom	167.29	5	tag-96	protein_coding	NON_SYNONYMOUS_CODING	F/S	tTc/tCc	0	+
I	1850251	C	G	SNP	Hom	350.74	10	tag-96	galactokinase	NON_SYNONYMOUS_CODING	D/E	gaC/gaG	1	
I	1850423	*		INS	Hom	151.46	8	tag-96		UTR_3_PRIME: 19 bases from CDS				
I	1874807	T	G	SNP	Hom	205.74	6	tub-2	Tubby-related	NON_SYNONYMOUS_CODING	V/G	gTt/gGt	0	+
I	1879747	A	G	SNP	Hom	194.91	6	tub-2		NON_SYNONYMOUS_CODING	T/A	Act/Gct	0	
I	1894681	C	T	SNP	Hom	144.86	6	Y71G12A.4	protein_coding	NON_SYNONYMOUS_CODING	G/E	gGg/gAg	0	
I	1910488	T	G	SNP	Hom	38.39	2	trpp-10	protein_coding	NON_SYNONYMOUS_CODING	F/L	ttT/ttG	1	+
I	1917998	A	C	SNP	Hom	482.79	13	trpp-10		NON_SYNONYMOUS_CODING	Q/H	caA/caC	1	
I	1941145	A	C	SNP	Hom	164.26	5	Y51F10.4	protein_coding	NON_SYNONYMOUS_CODING	T/P	Acg/Ccg	0	+
I	1941368	A	G	SNP	Hom	189.28	6	Y51F10.4		NON_SYNONYMOUS_CODING	E/G	gAa/gGa	0	
I	1945085	*		DEL	Hom	114.12	9	Y51F10.4		UTR_3_PRIME: 51 bases from CDS				
I	1950653	*		DEL	Hom	305.02	18	spe-48	ubiquitin-associated protein	UTR_3_PRIME: 122 bases from CDS				
I	1953467	T	C	SNP	Hom	228.43	7	spe-48		NON_SYNONYMOUS_CODING	K/E	Aaa/Gaa	0	
I	1958466	C	T	SNP	Hom	434.73	13	spe-48		UTR_5_PRIME: 10 bases from TSS				